

A Bio-Inspired Algorithm and Foldable Robot Platform for Collective Excavation

by

Zz Mae Haggerty

A Thesis Presented in Partial Fulfillment
of the Requirements for the Degree
Master of Science

Approved July 2018 by the
Graduate Supervisory Committee:

Spring Berman, Chair
Daniel Aukes
Hamid Marvi

ARIZONA STATE UNIVERSITY

August 2018

ABSTRACT

Existing robotic excavation research has been primarily focused on lunar mining missions or simple traffic control in confined tunnels, however little work attempts to bring collective excavation into the realm of human infrastructure. This thesis explores a decentralized approach to excavation processes, where traffic laws are borrowed from swarms of fire ants (*Solenopsis invicta*) or termites (*Coptotermes formosanus*) to create decision rules for a swarm of robots working together and organizing effectively to create a desired final excavated pattern.

First, a literature review of the behavioral rules of different types of insect colonies and the resulting structural patterns over the course of excavation was conducted. After identifying pertinent excavation laws, three different finite state machines were generated that relate to construction, search and rescue operations, and extraterrestrial exploration. After analyzing these finite state machines, it became apparent that they all shared a common controller. Then, agent-based NetLogo software was used to simulate a swarm of agents that run this controller, and a model for excavating behaviors and patterns was fit to the simulation data. This model predicts the tunnel shapes formed in the simulation as a function of the swarm size and a time delay, called the *critical waiting period*, in one of the state transitions. Thus, by controlling the individual agents' behavior, it was possible to control the structural outcomes of collective excavation in simulation.

To create an experimental testbed that could be used to physically implement the controller, a small foldable robotic platform was developed, and its capabilities were tested in granular media. In order to characterize the granular media, force experiments were conducted and parameters were measured for resistive forces during an excavation cycle. The final experiment verified the robot's ability to engage in excavation and deposition, and to determine whether or not to begin the critical

waiting period. This testbed can be expanded with multiple robots to conduct small-scale experiments on collective excavation, such as further exploring the effects of the critical waiting period on the resulting excavation pattern. In addition, investigating other factors like tuning digging efficiency or deposition proximity could help to transition the proposed bio-inspired swarm excavation controllers to implementation in real-world applications.

*To my mother and sister, and to anyone who's ever had to make hard decisions for
the future they deserved*

ACKNOWLEDGEMENTS

I would first like to acknowledge Dr. Berman, who has been a strong supporter of my interest in bio-inspired collective excavation since I joined her lab as an undergraduate in 2015. I will miss our meetings and thoughtful exchanges of ideas.

I'd like to thank Dr. Aukes for introducing me to Foldable Robotics, which continues to capture my imagination while working on mechanism designs. I hope to continue my work with folding features well into my own career and personal projects.

I would like to also thank Dr. Marvi for showing me the field of bio-inspired robotics, which brought a new creative level to my perspective of engineering design. Combining my love of biology and robotics was a profound experience in my graduate career.

I am also indebted to Dr. Pavlic and Dr. Pratt from the School of Life Sciences for always pointing me in the right direction when I was curious about social insect behaviors. I could never have navigated such a broad multi-disciplinary topic without their help.

I'd also like to thank my friends who kept me from my work. You know who you are.

And finally I would like to remember my feline companion, Lou, who held on through my college career to the old age of eighteen before passing away during the last month of my masters. I hope there are paper bags in cat heaven.

TABLE OF CONTENTS

	Page
LIST OF FIGURES	vii
CHAPTER	
1 INTRODUCTION	1
1.1 Literature Review	3
1.2 Outline of the Thesis and Project Goals	5
2 MOTIVATION: THREE PERSPECTIVES	7
2.1 Construction Applications	7
2.2 Search and Rescue Operations	8
2.3 Extraterrestrial Applications	9
3 ALGORITHM DESIGN	10
3.1 Collective Excavation Behaviors in Social Insects	10
3.1.1 Construction	13
3.1.2 Search and Rescue	14
3.1.3 Space Exploration	15
3.2 The Critical Waiting Period	16
3.3 Non-dimensional Metrics for Evaluating Efficiency	18
4 SIMULATION DESIGN	20
5 SIMULATION RESULTS	25
6 EXPERIMENT DESIGN	32
7 GRANULAR MEDIA CHARACTERIZATION	35
7.1 Granular Media Selection Process	35
7.2 Force Experiments	37
8 ROBOTIC PLATFORM	40
8.1 Experimental Goals	41

CHAPTER	Page
8.2 Overview of Foldable Robotics	42
8.3 Motor Selection.....	45
8.4 Mechanism Design Evolution	47
8.5 Final Design	51
8.6 Manufacturing Process and Part Files	52
8.7 Code Logic.....	54
9 EXPERIMENTAL RESULTS	55
9.1 Locomotion	55
9.2 Transition.....	56
9.3 Excavation	57
9.4 Deposition	57
9.5 Discussion.....	58
10 CONCLUSION AND FUTURE RESEARCH.....	61
10.1 Conclusion	61
10.2 Future Goals	62
REFERENCES	63
APPENDIX	
A NETLOGO CODE	65
B ARDUINO CODE.....	70

LIST OF FIGURES

Figure	Page
1.1 Dr. Walter Tschinkel and an aluminum cast of the <i>Pogonomyrmex badius</i> nest [Tschinkel (2004)]	2
3.1 Examples of excavating agents, excavation faces, and areas for deposit in nature and in construction. Images borrowed from Ant (2018) and Exc (2018)	10
3.2 Finite state machine of robot during construction projects.....	14
3.3 Finite state machine of robot during search and rescue operations.....	15
3.4 Finite state machine of robot during extraterrestrial exploration.	16
3.5 Final, general finite state machine of robot during excavation processes.	17
4.1 (1) The NetLogo world after setup, with labels for each agent and patch state. (2) Algorithm flow.....	20
4.2 GAV values shown on each patch, along with the corresponding agent states for each range of values.....	22
4.3 NetLogo interface design	23
5.2 Exponentially decaying functions fitted to simulation data on expansion level vs. CWP for populations of 2, 10, and 50 agents	26
5.3 Exponentially decaying functions fitted to simulation data on expansion level vs. CWP for populations of 100, 150, and 200 agents	26
5.4 Plots of negative relationship between agent productivity and CWP ...	29
5.1 Examples of excavation patterns after 2000 time steps in the NetLogo simulations for different CWPs and population sizes	31
6.1 Sloped experimental test bed filled with granular media for excavation.	34
7.1 Examples of different spherical granular medias and their robot weight/volume ratio.	35

Figure	Page
7.2 Dried peas were ultimately selected for excavation materials due to their low cost, low density and uniformly spherical shape.	36
7.3 (1) Solidworks models for test stand holding motor and resistive force sensor. (2) Actual test bed setup using wheel bracket, whег design, power supply and Arduino Uno.	37
7.4	39
8.1 (1) The very first acrylic prototype, featuring an IR sensor and 3D printed whегs with a foldable chassis (2) The second posterboard prototype, with stabilizing mandibles, forward facing IR sensor, actively sensing media carriage and foldable whегs (3) Final acrylic and fabric prototype, featuring a suspension system, dumping mechanism, actively sensing media carriage, foldable whегs and two IR sensors	40
8.2 Final excavating and locomoting mechanism	41
8.3 Initial origami chassis ideas, made of scrap paper and cardboard	43
8.4 Example of a 5 layer foldable hinge	44
8.5 Example of the five layers before being adhered and cut out	45
8.6 Free Body Diagram for a two-linked whег mechanism as it rotates through granular media	45
8.7 Whег trajectory plot from Python script	46
8.8 Motor Torque-Speed-Efficiency Curve	47
8.9 The locomoting (left) and excavating (right) modes of the first prototype	47
8.10 Stabilizing mandible mechanism made completely out of laminate parts	48
8.11 Examples of different foldable whегs attached to wheel brackets.	48

Figure	Page
8.12 Cardboard foldable whег design from second prototype in locomoting (left) and excavating (right) modes.	49
8.13 Final acrylic whегs with reinforcing fabric flex layer. Locomoting mode (center) and excavating mode (right). Rotations are limited by the whег material thickness during excavation.	50
8.14 Servo-actuated dumping mechanism from final design.....	51
8.15 Final robot design	51
8.16 Cut DXF files for final set of 10 whегs.	53
8.17 Cut DXF files for final chassis	54
9.1 The robot in position for (1) Roaming (2) Excavating (3) Depositing ..	55
9.2 Different headings of robot during locomotion.....	56
9.3 Examples of robot stuck on edge of granular media	57
9.4 Excavation patterns left by robot and LED activation with full chassis .	58
9.5 Robot depositing outside of arena	59

Chapter 1

INTRODUCTION

Traditional machinery used for excavation purposes is highly inefficient [Iai (2011)], lacks robustness [Lislerud (1988)], and always leaves a large footprint on the environment it works in [Siciliano and Khatib (2008)]. Yet in nature, swarms of some species of insects will work together so efficiently at excavation that they are often seen as an individual complex organism executing a single task. If the main objective of swarm robotics is to develop robust collectives of robots that will execute complex behaviors using simple sets of rules, couldnt these same rules be applied to a swarm excavating agents to improve the current state of digging machinery? Bio-inspired swarm excavation in robotics has real world applications that could revolutionize construction, space exploration, and rescue missions by increasing efficiency, being compact and resilient enough to travel, and expediting the extrication process in search of survivors in disaster zones. Excavation is a difficult topic to study, due to the fact that the process occurs underground and out of sight. Once describing the challenges faced by those attempting to study excavation, Dr. Stephen Pratt at Arizona State University told a story about how one lab was able to replicate excavation conditions for a swarm of termites, however the termites would repeatedly block the observer's viewing window with mud when an attempt to watch their behavior was made [Pratt (2017)]. It is well known in entomology circles that termites dislike being watched and will do everything possible to prevent the viewer from seeing them work. In studies of insect excavation, it seems that one of two approaches are always used:

1. To observe the individual insects' behavior during excavation.

2. To observe the nest architecture changes during excavation.

This thesis aims to bridge the gap between these two methodologies and show that by controlling aspects of the behavior of individual agents, it is possible to control the excavation geometry produced by a swarm of these agents.



Figure 1.1: Dr. Walter Tschinkel and an aluminum cast of the *Pogonomyrmex badius* nest [Tschinkel (2004)]

In regards to understanding the progression of insect nest architecture during excavation, this thesis uses the work of Dr. Walter Tschinkel, Dr. Jean-Louis Deneubourg, and Dr. Guy Threlauz. Tschinkel is best known for his aluminum casts of ant nests (once the subject of viral videos seen across multiple social media platforms), which allowed the in-depth study of the nest structure as it relates to a colony's collective digging effort [Tschinkel (2004)]. An example of one of his aluminum casts is seen above in Figure 1.1. Deneubourg is best known for studying self-organization in animal societies, with a focus on collective decision i.e. how a large group can make decisions that are beyond the scope of an individual agents cognitive ability [Camazine *et al.* (2003)]. Finally, Threlauz is well known for his work on collective

insect behavior, including classification of the architecture of termite nests [Camazine *et al.* (2003)]. Most of the work in this thesis that is inspired by termite excavation behavior draws on studies from from Dr. Paul Bardunias' lab at at University of Florida. He has done thorough research on this topic, observing queue creation during excavation to quantifying variations in individual termites' behavior during excavation [Bardunias and Su (2010)], and has even been able to characterize branching patterns by studying the opposing headings of excavating and depositing termites [Bardunias and Su (2009)]. A bio-inspired approach to collective excavation presents a novel contribution to the field swarm robotics, since it addresses an understudied scenario: the control of a swarm in a confined environment in which the available area to be traversed is constantly changing due to the activities of the agents. As in other swarm robotics problems, the agent behavioral rules must be designed such that the collective efficiently completes a desired task.

1.1 Literature Review

The most popular example of excavation in robotics is without a doubt the NASA Robotic Mining Competition (RMC). This competition brings in over 50 college teams to mine precious icy regolith (which is a compound similar to the soil found on the moon) [rmc (2018)]. The rubrics for the competition ensure that only one robot is created per team, so the competition's contributions to the study of excavation remain limited to mechanisms and individual excavation algorithms. In addition to a cash prize to the winning team, the designs brought forward in this annual competition have helped to inspire designs implemented on future mining missions. The robot in this thesis differs from those in the NASA RMC because it is designed to excavate small parcels of coarse granular media, and it is intended to be a platform that is used in swarm applications.

Current robotic swarm solutions to excavation include the Artificial-Neural-Tissue (ANT) Controllers developed by Thangavelautham *et al.* (2017), the robophysical work done at Georgia Tech involving excavation in confined environments by Linevich *et al.* (2016), and the TERMES robotic platform by the Wyss Institute at Harvard by Petersen *et al.* (2011). In [Thangavelautham *et al.* (2017)], the ANT Controller used only one global fitness function and a set of allowable basis behaviors to exhibit swarm intelligence concepts of stigmergy, templates, and self-organization as it applied to excavation. The simulation and experiment was tailored to assist with excavation processes on the moon (again specifically excavating regolith) in small swarms. The algorithm was tested on the commercially available four-wheeled Argo Rover in swarms ranging from 1-5 robots, however one drawback to the algorithm was it's lack of scalability to swarms of different sizes. When the swarm was decreased down to only one robot, there was a large degradation in system performance because the robot controllers had evolved to depend on cooperative actions [Thangavelautham *et al.* (2017)]. This thesis aims to use a simple, unchanging set of excavation laws followed by identical agents, each equipped with novel excavation hardware designed to excavate in a coarse granular media.

The excavation research done by the Goldman Lab at Georgia Tech focused on the density of robots working in a confined tunnel, and established that larger groups of robots were more prone to traffic jams with fewer instances of individual robot excavation [Linevich *et al.* (2016)]. Despite these factors, the rate of excavation was still improved in larger groups and it was determined that the success of collective robotic excavation depends on the size of the swarm and the width of the tunnel. A new differential-drive robotic platform was designed and equipped with a low cost camera system, a gyroscope, and a magnetometer. A pheromone trail was simulated using a line following algorithm. The results of this study did not consider the final

excavated structure, and the digging mechanism used in their experiments was a mandible gripper [Linevich *et al.* (2016)]. The robotic platform designed in this thesis excavates using a dredge inspired mechanism, and the algorithm designed provides important insights to the changes in the final nest architecture. The TERMES robot developed by the Wyss Institute at Harvard University is in fact a platform for testing collective construction rather than excavation; however it bears mentioning in this thesis because it uses similar termite-inspired algorithms [Petersen *et al.* (2011)]. Also this is the first robotic platform to use a mechanism called a "wheg" or "wheel-leg," which is a locomotion mechanism capable of traversing over rough terrain and even loose granular media [?]. This mechanism is a mechanism that was later implemented into the final robotic platform in this thesis.

With respect to previous work on robotic excavation, additional differences in the work of this thesis include the fact that the experiments conducted handle a characterized loose granular media, the excavation behavior is described by a simple control algorithm, and the final robotic platform incorporates aspects of foldable robotics and has a bio-inspired sensing capability.

1.2 Outline of the Thesis and Project Goals

This thesis will first summarize the existing work on swarm excavation, focusing on biological studies that highlight either the evolution of a colony's nest architecture or the nature of individual agents' behaviors as they relate to excavation. Then it will describe the design of bio-inspired algorithms for swarm excavation and simulations of these algorithms in NetLogo [Wilensky and Rand (2015)]. The data from these simulations will then be used to characterize the relationships between the size of the swarm and the amount of material excavated, the final excavated structure, and a controllable time delay parameter called the "critical waiting period." The usefulness

of these models will be evaluated as they relate to the following infrastructure problems: Construction, Search and Rescue Operations, and Space Exploration. Then, methods for selecting the granular media for the experimental testbed will be described, as well as the results of a force test analysis of the granular media with a potential wheel design for the robotic platform. After that, the design evolution for a small-scale foldable robotic excavator will be discussed. Finally, the results of both the NetLogo simulations and robot tests in granular media will be discussed, along with the scope of future work to be done with this robotic platform and swarm excavation models. This thesis ultimately aims to highlight the effectiveness of bio-inspired collective excavation strategies for robotic swarms as applied to human infrastructure problems.

Chapter 2

MOTIVATION: THREE PERSPECTIVES

Replacing Tunnel Boring Machines (TBMs) in several human infrastructure problems could ultimately save money, lives and manpower. In this section, many of the issues faced by modern construction, search and rescue, and extraterrestrial exploration strategies are discussed and compared to the benefits of switching to a decentralized robotic swarm.

2.1 Construction Applications

Tunnel Boring Machines are the industry standard for excavation procedures, however they are very costly and lack the efficiency that could be delivered from a bio-inspired robotic swarm. By comparing the energy efficiency of various systems, Iai (2011) reported that the amount of Joules of energy needed to excavate one cubic meter of rock by TBMs totaled 3.0×10^8 . Comparatively, a swarm of ants excavating sand expends 1.2×10^4 Joules of energy per cubic meter of sand excavated [Iai (2011)], which amounts to ant excavation being about 10,000 times more efficient than Tunnel Boring Machine excavation. TBMs require a huge number of workers to keep running, and move incredibly slowly. To put it into perspective, a snail is effectively 14 times faster than a soft-soil TBM [Bor (2017)]. The future of traffic in densely populated cities is dependent on 3D solutions, and Elon Musk's hyperloop project is looking to solve that through The Boring Company [Bor (2017)]. They mention that tunnels are necessary in city construction because there is no practical limit to how many layers of tunnels can be built, they are weatherproof, and the construction operations are invisible to those on the surface [Bor (2017)]. In regards to the state of current

tunneling projects, there has been virtually no investment in tunneling research and development and the construction industry is one of the only sectors in the United States that has not improved its productivity in the last 50 years [Bor (2017)]. While the Boring Company looks to improve upon the existing platform of TBMs, maybe it's time that a new technology attempts to tackle tunneling efforts. The current state of TBM processes are not independent of the occasional fiasco, with the New York Times mentioning how the tunnel that currently runs under second avenue in New York City to this day remains the most expensive mile of subway track on Earth, capping out at a cost of 2.5 billion USD [Rosenthal (2017)]. Finally, the working conditions for those operating TBMs are cramped and frequently very dangerous. Between the years of 1993 to 2017, 35 total fatalities have been reported as a result of TBMs [TBM (2018)]. By switching from one large machine to a swarm of independent excavating agents, costs and manpower would be significantly reduced and tunnel construction could be more easily implemented into construction as cities grow.

2.2 Search and Rescue Operations

Swarms capable of bio-inspired excavation could enable the rescue of many more survivors in the event of a disaster. The Handbook for Robotics mentions that most of the survivors of urban disasters (80 %) are surface victims (meaning they were lying on the surface of the rubble or at least easily visible by someone assessing the damage). Sadly only 20% of survivors of urban disasters come from the interior of the disaster zone, even though the interior is where most of the victims are located [Siciliano and Khatib (2008)]. This provides urgent motivation for robots that can explore deep within a collapsed area [Siciliano and Khatib (2008)]. In disasters like the Oklahoma City Bombing, life support could have been provided by transporting supplies through narrow tubing during the long periods that victims are waiting to be

rescued [Siciliano and Khatib (2008)]. Consider this: if ants and termites are capable of excavating large, elaborate underground nests, couldn't a swarm of robots excavate a nest into rubble to hopefully search the entire area below more efficiently without having to remove all of the rubble? This could be a quick and efficient way to find the victims and potentially provide medical treatment. When disasters strike, it may be far more beneficial to allow a robotic swarm to assess the damage while being able to cover ground in a manner that helps find survivors from within the rubble.

2.3 Extraterrestrial Applications

A bio-inspired excavating swarm is potentially a very practical system for excavating in extraterrestrial planetary environments due to the low weight of the robots and decentralized control architecture. Aside from NASA's Robotic Mining Competition, several space exploration companies are interested in studying extraterrestrial soil properties, but existing technology is not always adaptable to changing conditions. Ants themselves are able to excavate over a large range of different soil sizes and moisture contents, and thus offer a paradigm for designing a highly robust distributed system for exploration [Espinoza and Santamarina (2010)]. Furthermore, a swarm of robots would be well-suited to set up stations autonomously before any humans have to take a risky interplanetary journey. In terms of weight, TBM's can weigh upwards of 5,000 pounds [Lislerud (1988)], meaning that it would be much more efficient to transport a lightweight swarm through space than to attempt to move one gargantuan piece of machinery. Finally, if there is only one machine sent out to complete an excavation task and that machine breaks, the entire operation fails. Interplanetary exploration can benefit from the robustness of robotic swarms in the presence of failures and errors of individual agents, in addition to saving fuel costs and complying with size constraints.

Chapter 3

ALGORITHM DESIGN

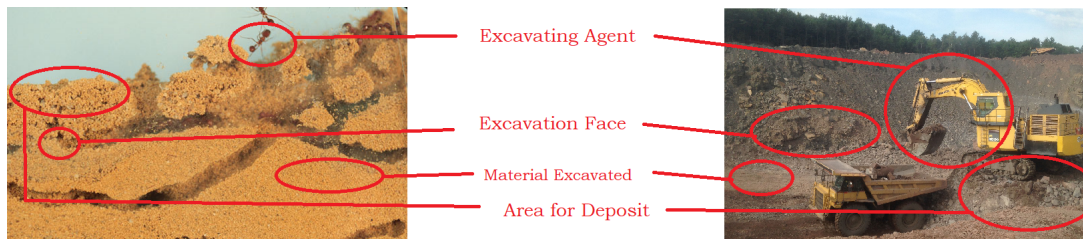


Figure 3.1: Examples of excavating agents, excavation faces, and areas for deposit in nature and in construction. Images borrowed from Ant (2018) and Exc (2018)

Regardless if by animal or machine, excavation processes will always involve an excavating agent, an excavation face and an area for deposit. The excavating agent will have an efficiency as it relates to the amount of material excavated, the excavation face will determine the overall structure of the final result, and the proximity of the area for deposit will effect the efficiency and final structure. These elements were taken into consideration during the algorithm design as they apply to excavation across all different platforms. This section will explore different species' excavation strategies in order to formulate an executable algorithm by a robotic swarm, specifically considering different approaches for construction, search and rescue, and extraterrestrial exploration.

3.1 Collective Excavation Behaviors in Social Insects

After reviewing pertinent studies on excavation behaviors in termite (*Coptotermes formosanus*), fire ants (*Soloenopsis invicta*), and argentine ants (*Linepithema humile*

mayr), the following traffic laws and observations were designated as particularly useful for collective excavation applications:

1. Net flux of ants exiting an arena was improved by partial obstructions to exit. (*Linepithema humile mayr*) [Burd *et al.* (2010)]
2. Creating a Global Away Vector (GAV). (*Coptotermes formosanus*) [Bardunias and Su (2009)]
3. Depositing material inside of a tunnel opposite the direction of the GAV to cause branching in the direction of the GAV. (*Coptotermes formosanus*) [Bardunias and Su (2009)]
4. In the case of a traffic jam, agents will wait in a queue as they dig and start digging along the wall of the tunnel after a critical period. (*Coptotermes formosanus*) [Bardunias and Su (2009)]
5. Tunnels widths are proportional to worker size. (*Soloenopsis invicta*) [Gravish *et al.* (2012)]
6. Material is always deposited on the surface or outside of the excavation arena. (*Soloenopsis invicta*) [Gravish *et al.* (2012)]
7. Only 20-30 % of groups participated in digging at any time, and remaining workers aggregated on the outskirts of the arena. (*Soloenopsis invicta*) [Gravish *et al.* (2012)]
8. Varying worker size improves excavating efficiency. (*Soloenopsis invicta*) [Gravish *et al.* (2012)]

9. Termites response to tactile information (acquired through antennae) helps them to form a queue for excavating (related to digging pressure). (*Coptotermes formosanus*) [Bardunias and Su (2010)]
10. Termites only need to know if they are at the digging surface, or along the tunnel wall. If at surface, termite digs. If at wall, termite waits for a critical period of time and then digs. (*Coptotermes formosanus*) [Bardunias and Su (2010)]
11. Tunnel depth increases with soil moisture. (*Soloenopsis invicta*) [Gravish *et al.* (2012)]
12. Vertex degree (branching rate) increases as soil moisture and soil coarseness increases. (*Soloenopsis invicta*) [Espinoza and Santamarina (2010)]
13. Biomechanics for small particles include 1) anchoring 2) compression and 3) transport (considered formation i.e. pellet formation). (*Soloenopsis invicta*) [Espinoza and Santamarina (2010)]
14. Biomechanics for large particles include 1) particle grasp 2) retreat (considered pulling). (*Soloenopsis invicta*) [Espinoza and Santamarina (2010)]
15. Ants actively use their antennae to help adjust their load as they carry it out of a nest. (*Soloenopsis invicta*) [Espinoza and Santamarina (2010)]

Based on these traffic rules and observations, three finite state machines were developed as controllers for robots in an excavating swarm to implement the priorities and excavation laws most relevant to the pre-selected infrastructure problems. Each different approach first outlines the major challenges for the problem, and then defines traffic laws that will produce the desired outcome.

3.1.1 Construction

Challenges to consider when designing an algorithm for construction include:

1. Energy Efficiency
2. Collaboration Between Robots

The excavation laws that are most relevant to these challenges are:

- Creation of a GAV *Coptotermes formosanus* (Rule 2)
- Varying worker size to increase efficiency *Soloenopsis invicta* (Rule 8)
- Queue creation for excavation, incorporating a critical waiting period *Coptotermes formosanus* (Rule 4)
- Biomechanics for particles *Soloenopsis invicta* (Rule 13)

Taking these goals and biological phenomena into consideration, the following finite state machine was devised as a controller for a robot in a swarm performing excavation in construction applications.

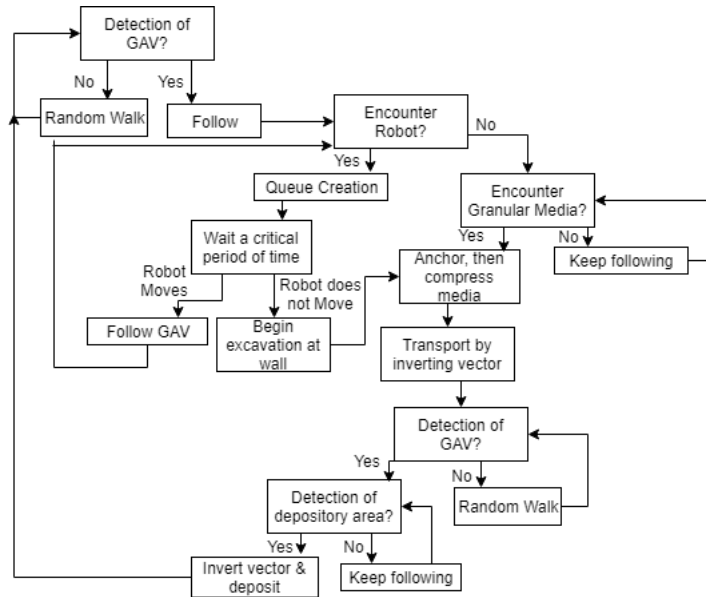


Figure 3.2: Finite state machine of robot during construction projects.

3.1.2 Search and Rescue

Challenges to consider while designing an algorithm for search and rescue include:

1. Boundary Coverage
2. Excavation Rates

The excavation laws that are most relevant to these challenges are:

- Creation of a GAV *Coptotermes formosanus* (Rule 2)
- When collisions occur, robots will turn to head in opposite directions. Queue will be zero. *Coptotermes formosanus* (Rule 4)
- Net flux of ants exiting an arena is improved by partial obstructions near the exit. *Linepithema humile mayr* (Rule 1)
- Biomechanics for particles. *Soloenopsis invicta* (Rule 13)

Taking these goals and biological phenomena into consideration, the following finite state machine was devised as a controller for a robot in a swarm performing excavation for search and rescue operations.

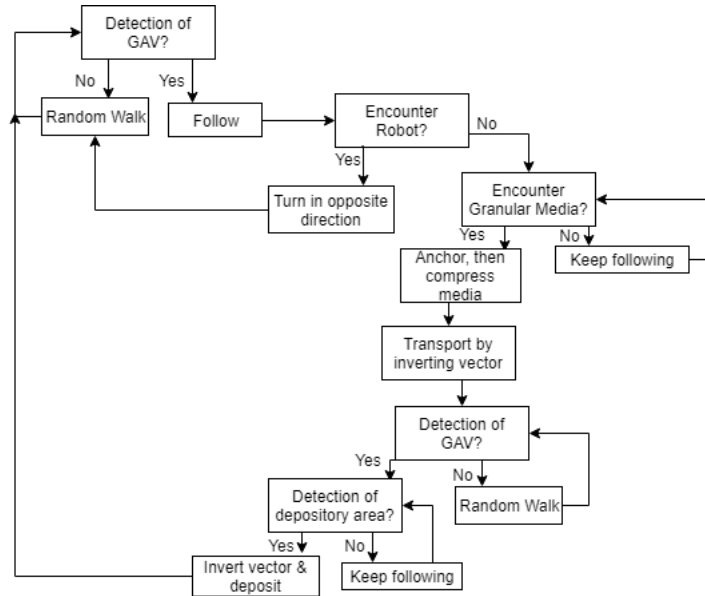


Figure 3.3: Finite state machine of robot during search and rescue operations.

3.1.3 Space Exploration

Challenges to consider while designing an algorithm for extraterrestrial exploration include:

1. Energy Efficiency
2. Boundary coverage

The excavation laws that are most relevant to these challenges are:

- Creation of a GAV *Coptotermes formosanus* (Rule 2)
- Only 20-30 percent of groups participate in digging at any time. *Soloenopsis invicta* (Rule 7)

- Queue creation for excavation, incorporating a critical waiting period *Coptotermes formosanus* (Rule 4)
- Tunnel depth increases/decreases as soil properties change. *Soloenopsis invicta* (Rule 11)
- Biomechanics for particles. *Soloenopsis invicta* (Rule 13)

Taking these goals and biological phenomena into consideration, the following finite state machine was devised as a controller for a robot in a swarm performing excavation for extraterrestrial exploration.

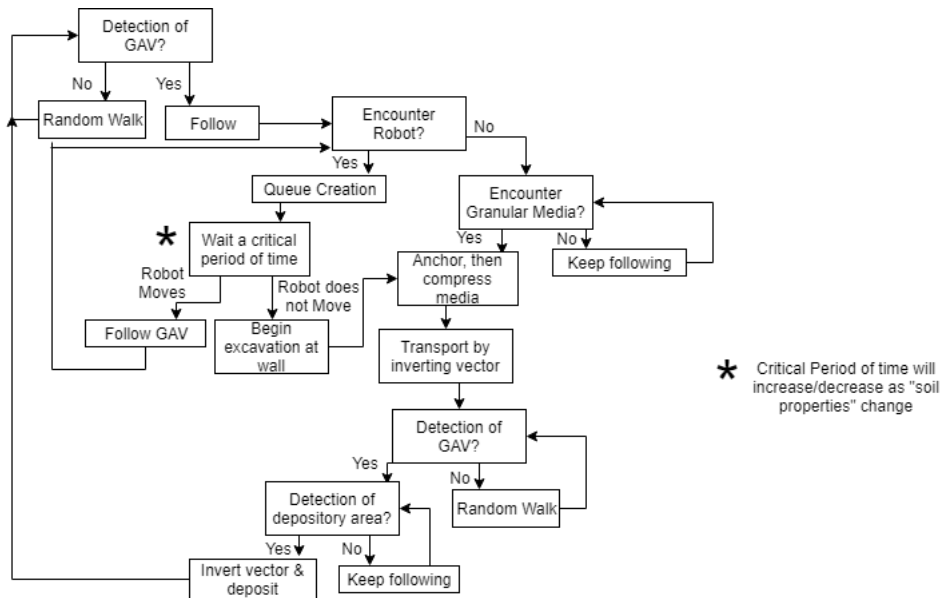


Figure 3.4: Finite state machine of robot during extraterrestrial exploration.

3.2 The Critical Waiting Period

After analyzing the processes outlined in each finite state machine, one excavation phenomenon that is present in all three infrastructure problems is the critical waiting period (CWP) described in law number 10. This behavioral law has major implications for the structural outcome of excavation, which is later quantified in this

As Barduinias puts it, the CWP creates digging pressure [Barduinias and Su (2009)], which is directly correlated to nest expansion. It eventually became apparent that excavation has a nearly identical finite state machine across each of the three scenarios, which means that a unique algorithm no longer needs to be designed per situation. Now, the same algorithm can be used, but tuning the CWP in each will yield different results as they cater to a desired final outcome and it's priorities. The simulation used in this thesis aims to model the effects of the critical waiting period as it relates to excavation processes.

3.3 Non-dimensional Metrics for Evaluating Efficiency

When calculating excavation efficiency for different robotic platforms, two separate factors must be considered: the amount of soil excavated and the power needed to excavate it. In order to make a fair comparison of different excavating systems, the following non-dimensional efficiency metric was developed:

$$\text{Efficiency} = \frac{\left(\frac{E_{cycle}}{E_{max}} \right)}{\left(\frac{M_{parcel}}{M_{excavator}} \right)}$$

where

$$E_{cycle} = \text{energy required to complete one cycle}$$

$$E_{max} = \text{maximum amount of energy contained by excavator}$$

$$M_{parcel} = \text{average mass of a parcel of media excavated}$$

$$M_{excavator} = \text{mass of excavator}$$

Here, one excavation cycle includes phases of roaming, excavating a parcel, and depositing the parcel. M_{parcel} is defined as the average mass of a parcel excavated

by the robot, regardless of the granular media type. Note that an excavator that uses almost no energy over a cycle to retrieve a small parcel could have the same efficiency score as an excavator that uses a lot of energy to retrieve a large parcel. According to the definition of the efficiency metric, a robotic excavator can achieve optimal efficiency by excavating a large amount of material using little energy. The goal of the efficiency equation is to minimize the numerator while maximizing the denominator, so a lower score is considered more efficient. The final goal of excavation is to excavate more material with less energy, which is explicitly defined here.

SIMULATION DESIGN

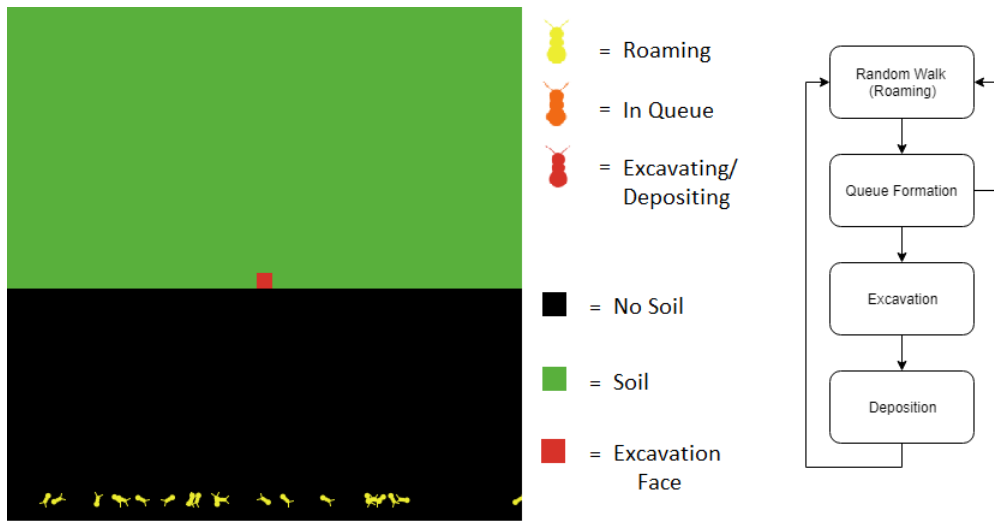


Figure 4.1: (1) The NetLogo world after setup, with labels for each agent and patch state. (2) Algorithm flow.

For simulation purposes, the agent-based NetLogo software was used to quickly develop models for a swarm of termite-inspired robots with adjustable population sizes and varying critical waiting periods. This software is capable of generating visual results of the final outcome of the excavated structure, which enables the quantification of expansion levels, defined as the number of new excavation faces formed, per swarm size and critical waiting period length. In order to measure a swarm's efficiency, the simulation tracked excavated material leaving the arena per individual agent. In order to characterize the final excavated structure, the simulation showed the number of new excavation faces formed (i.e. expansions) as they varied with swarm size and critical waiting period.

As defined by [Wilensky and Rand (2015)], the model created is a *phenomena-based model*, which is designed to reproduce a known target phenomenon (in this case, high and low expansion during excavation). The goal of phenomena-based modeling is to build a model that will result in the chosen reference pattern, where a high waiting period creates a simple tunnel-like excavation and a low waiting period creates an expansive one. The question to answer by the creation of this model is: “How can the critical waiting period be defined for a swarm of a particular size to achieve a desired level of expansion during excavation?” By collecting simulation data and identifying its dependence on the tunable parameters of the system, it is possible to relate excavation patterns across swarm sizes to varying waiting periods. The end goal is to select a particular population size and desired expansion level and use it to calculate the necessary waiting period.

Incorporating the roaming, excavating, and depositing phases of excavation, a flowchart for the individual agents’ behavior was designed (Figure 4.1). In the same figure is an example of the different possible states that individual agents can have, where yellow means the agent is roaming, red means the agent is excavating or depositing, and orange means the agent is waiting in a queue. Three different states for the environment underneath the agents were also defined, where black means there is an absence of soil (and it can be traversed by an agent) and green means there is soil present (and it cannot be traversed). Since excavation is only to be initiated at an excavation face, red spots in the environment indicate the presence of an excavation face.

In order to implement the existence of a GAV [Bardunias and Su (2009)], each patch underneath an agent was assigned a numerical value. The area closest to the bottom of the arena started at 1, and the values increased along the y-axis of the arena until the final GAV value was reached at 16.

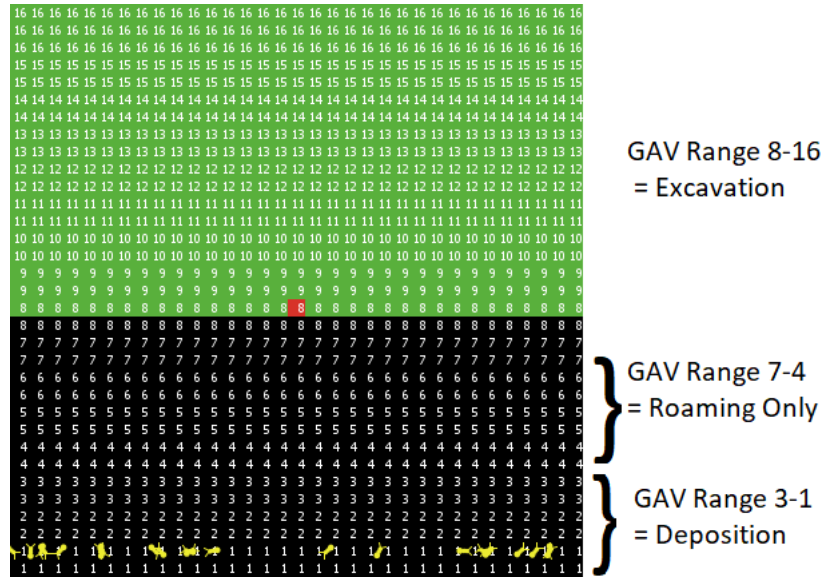


Figure 4.2: GAV values shown on each patch, along with the corresponding agent states for each range of values

The NetLogo program begins by setting up the empty (black) and soil-filled (green) patches in the arena, and then placing a single excavation face (red) at the edge of the soil patch. Then, the values of the GAV are assigned to each individual patch. A variable population size of agents is created (which is tunable by the slider bar shown in Figure 4.3), and the agents are placed randomly along the x direction at a single y-coordinate location at the bottom of the arena. Then, a value for the CWP is chosen. Once the setup is complete, the simulation of the excavation process begins.

The code implements three phases: roaming, excavating, and depositing. The roaming phase starts with agents random-walking over empty patches and stepping backward over soil-filled patches. While roaming, an agent's state is also set to roaming (yellow) in order to track which agents are actively engaged in this phase. Then, when the agent enters a patch with a GAV value of 8 or higher (i.e., somewhere within the excavation area), a second block of code checks the agent's surroundings

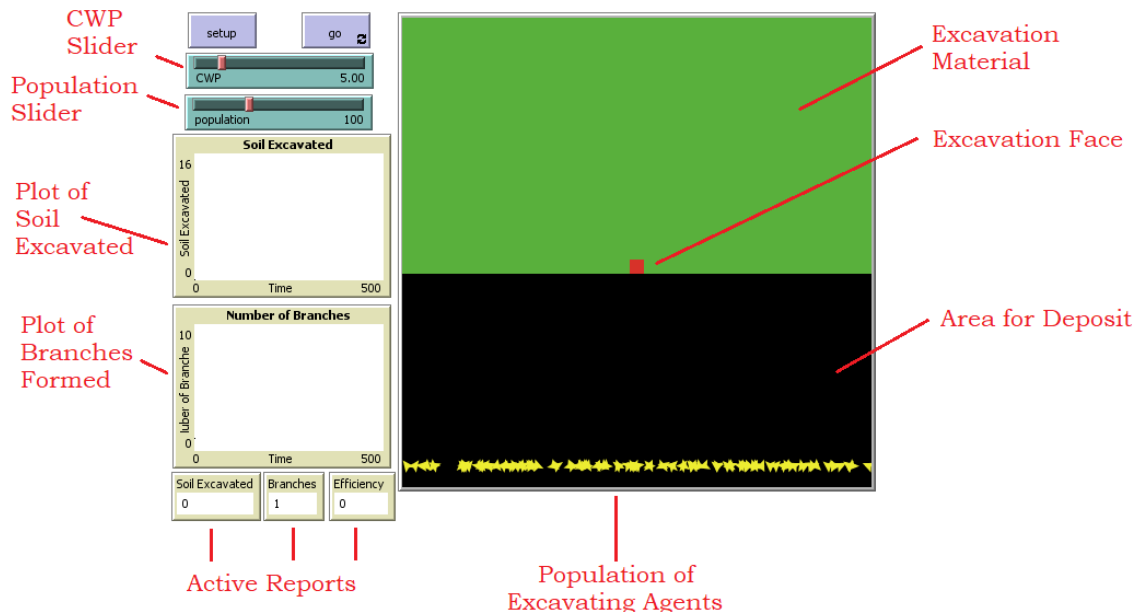


Figure 4.3: NetLogo interface design

(i.e., its neighboring 8 patches). If the agent is near another agent that is excavating (red), the first agent will change its color to orange and begin waiting in a queue. The agent waits for the duration of the critical waiting period (CWP), after which it checks its surroundings again. If there is no queue after the agent is finished waiting, it returns to the roaming state until it discovers an excavation face. On the other hand, if the agent is still in the queue, it randomly sets its heading left or right and creates a new excavation face at the nearest patch. Afterward, the agent transitions to the excavating state. Every time a new excavation face is created, a counter is incremented to track the instances of expansion of the excavated material.

If an agent encounters a patch that is an excavation face, the patch state is changed from an excavation face to an empty patch, and the soil-filled patch behind the changed patch turns into the new excavation face. During and after excavation, the agent changes its state from either roaming (yellow) or waiting in queue (orange) to excavating (red). Then, it begins depositing.

In the depositing phase, if the agent's state is excavating, it travels along black patches with decreasing GAV values until it reaches a patch with a GAV value less than 3. Once there, the black patch that the robot occupies turns to green to simulate deposition. The agent then returns to roaming, and the cycle starts over again.

In summary, the simulation data of interest consists of the amount of soil excavated, the instances of expansion (i.e., the creation of new excavation faces), and a visual rendering of the excavated structure after 2000 time steps.

Chapter 5

SIMULATION RESULTS

One of the benefits of using NetLogo for simulations is that the effects of CWP on expansion can be qualitatively observed. Figure 5.1 (at the end of this chapter) shows examples of final excavation patterns for five CWP values and six agent population sizes after 2000 time steps in the simulation trials. The figure illustrates that large populations with a low CWP produce wide tunnels and cavities, while all populations with a high CWP produce only narrow tunnels.

To track the degree of expansion of the excavated material in the simulations, the number of new excavation faces after 2000 time steps, defined as N_{exp} , was counted for each agent population size and plotted against the range of simulated CWPs. Then, a function was fitted to this data for each population size in order to predict the CWP necessary for a desired level of expansion during excavation. Figures 5.2 and 5.3 plot the average and standard deviations of the expansion level over five simulation trials for each population size and CWP value, along with the corresponding fitting functions, which are each approximated as a decaying exponential function.

For all of the population sizes, the functions asymptotically approached a value of 1 (or close to 1). This is an intuitive result, because there can never be an instance where the number of tunnels decreases below a value of 1.

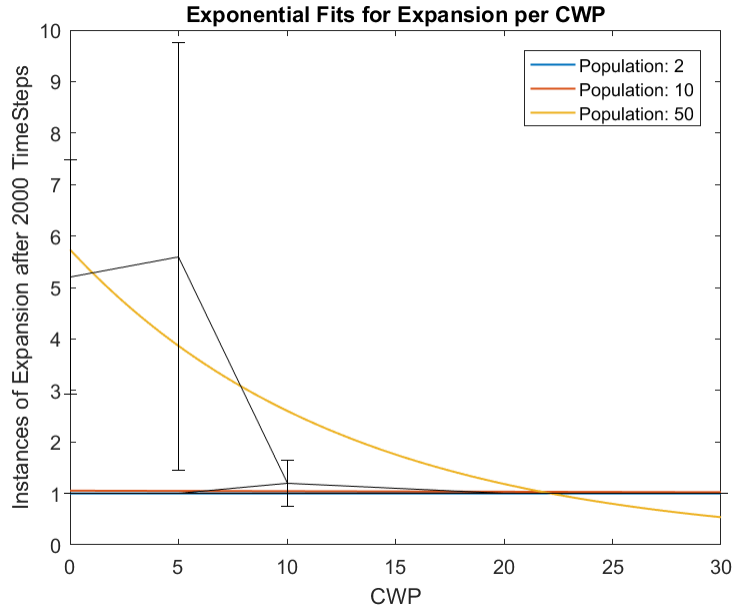


Figure 5.2: Exponentially decaying functions fitted to simulation data on expansion level vs. CWP for populations of 2, 10, and 50 agents

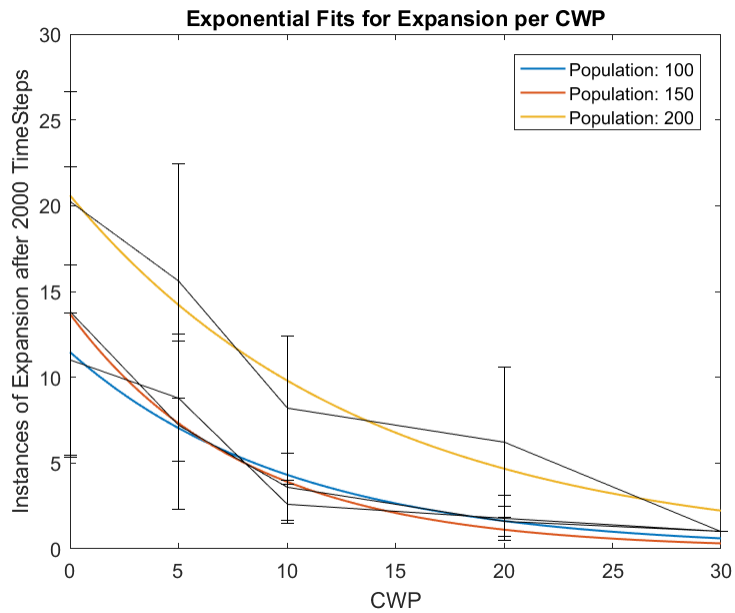


Figure 5.3: Exponentially decaying functions fitted to simulation data on expansion level vs. CWP for populations of 100, 150, and 200 agents

The exponential fitting function for each population size is given below, along with the coefficients determined for each fitting function and their R-squared approximation values:

$$N_{exp} = ae^{bCWP}$$

where

Population	a	b	R-squared
2	1.0000	0.0000	N/A
10	1.0530	-0.0010	0.0188
50	5.7360	-0.0789	0.7563
100	11.4700	-0.09759	0.9216
150	13.6900	-0.1251	0.8188
200	20.6000	-0.0741	0.9636

One of the goals of the simulation was to prove that it was possible to control the degree of expansion of the excavated material using only the CWP. The following formula for the CWP was derived from the fitted exponentially decaying functions,

$$CWP = \frac{\ln(N_{exp}) - \ln(a(N_a))}{b(N_a)}$$

where the functions $a(N_a)$ and $b(N_a)$ are shown here as explicit functions of the population size N_a . These functions can be approximated as linear functions of N_a , fit to the data in the table above:

$$a(N_a) = 0.0971N_a + 0.637$$

$$b(N_a) = -0.0008N_a - 0.006$$

This formula shows that it is possible to calculate the CWP necessary to produce a target number of instances of expansion with a given agent population size.

As shown in Figure 5.2, for a population of 2 agents, the CWP value did not have any effect on the expansion level of the excavated material. This is likely due to the size of the arena, since a small swarm in a large area will likely never interact with another agent in the arena and expand the tunnel width to accommodate more excavating agents. In the case of 10 agents, again the simulation data showed that almost no expansion beyond the formation of a single tunnel occurred regardless of CWP value; however, there was one instance at a CWP value of 5 where one extra excavation face was formed. While this data point was an outlier in the simulations, it is worth considering with respect to the effects of agent clustering. This occurrence likely happened because an agent was inside of the tunnel being excavated and interacted with another agent, starting a queue. This could explain why in small populations a non-zero CWP could actually encourage some expansion. This effect seemed to disappear in larger populations, however. For a population of 50 agents, it can be seen that the number of new excavation faces at zero CWP increased to approximately 5, and expansion stops (i.e., there is only one excavation face) at a CWP of 22.1, according to the exponential fitting function. For values of CWP below 22.1, the expansion level remains fairly low.

As shown in Figure 5.3, for a population of 100 agents, the number of excavation faces at zero CWP increases to approximately 11, and expansion stops at a CWP of 25. For small CWP between 0 and 5, a cavity begins to form behind the tunnel entrance. For a population of 150 agents, it can be seen that the number of excavation faces at zero CWP increases to approximately 13, and expansion stops at a CWP of 20.9. The same cavity formation occurs for CWP between 0 and 10. For a population of 200, the number of excavation faces at zero CWP is approximately 21, and expansion stops at a CWP of approximately 40.8. Cavity formation occurs at CWP between 0 and 10, and for a CWP of 20, the final excavated structure remains a narrow tunnel.

Figure 5.4 plots the agent productivity, defined as the average amount of soil excavated per agent over the duration of the simulation trials (and average values were used). The figure shows that agent productivity decreases as CWP increases, regardless of population size. This is due to the fact that if an agent is waiting, it is not contributing to excavation. Thus, agent productivity must be sacrificed if the objective is to excavate narrow tunnels.

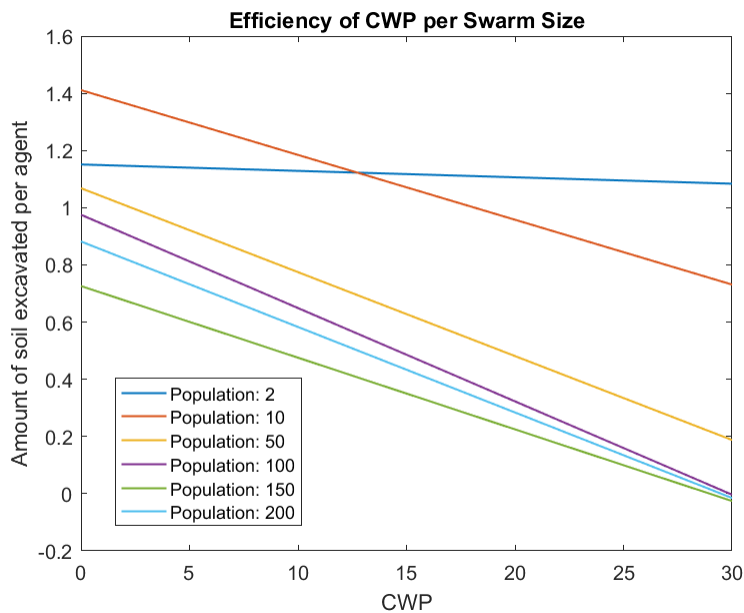


Figure 5.4: Plots of negative relationship between agent productivity and CWP

Due to the randomness in agents' motion while in the roaming state, there was a high degree of variation in data among simulation trials as indicated by the sizes of the error bars in Figures 5.2 and 5.3, which meant that the model would have benefited from more than five trials of data. had to be run in order to obtain an accurate characterization of the excavation behavior. Regardless, this random motion simulates the excavation law (Rule 7) that states that only 20-30% of ants participate in excavation at any given time, while the rest aggregate on the outside of the arena. If all agents were to directly follow the GAV into the excavation arena, the queue size

would require much a higher CWP and instances of expansion would skyrocket (not to mention efficiency would decrease dramatically).

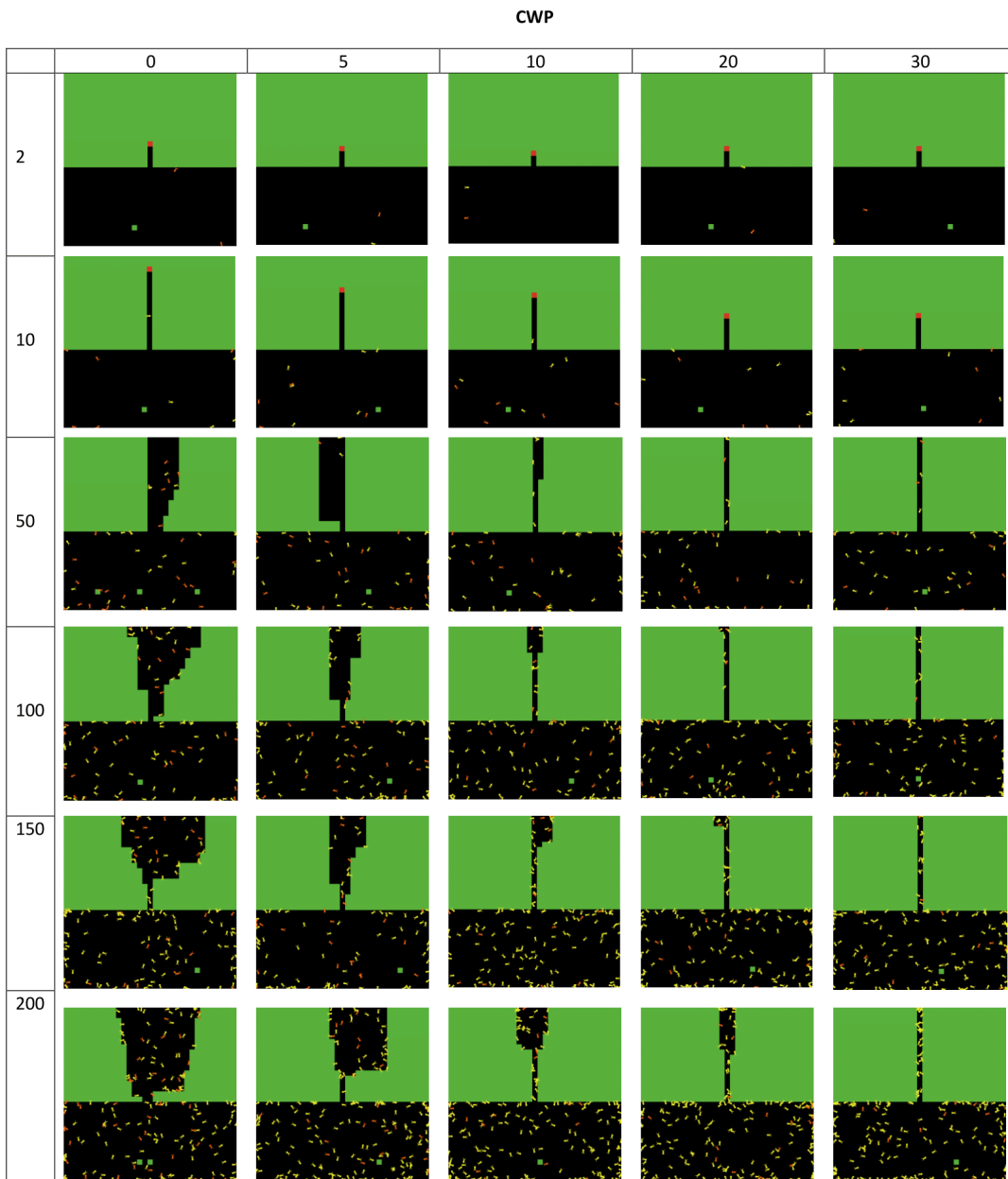


Figure 5.1: Examples of excavation patterns after 2000 time steps in the NetLogo simulations for different CWPs and population sizes

Chapter 6

EXPERIMENT DESIGN

The experimental setup involves a test bed of granular media and a singular excavating robotic platform. The goal is to verify that the platform has the sensing and actuator capabilities to follow the algorithm described in Chapter 5. This means that the robot must be capable of locomotion up to the granular media, then it must be able to reach the excavation face, then it must be able to excavate until its carrier chassis is full, and finally it must be able to deposit the granular media outside of the arena. Over the course of the excavation cycle, the robot must also be able to identify the presence of either an excavation face or of another robot. The presence of an excavation face will mean to begin excavating, and the presence of a robot will cause the robot to wait in queue and then check to see if it will begin to expand the tunnel.

The following factors were integrated into the design of the experiment:

- Creation of a Global Away Vector (GAV) *Coptotermes formosanus* (Rule 2)
- In the case of a traffic jam, termites will wait in a queue as they dig and start digging along the wall of the tunnel after a critical period. *Coptotermes formosanus* (Rule 4)
- Material is always deposited on the surface (outside of excavation arena). *Solenopsis invicta* (Rule 6)
- Termites response to tactile information helps them to form a queue for excavating (as related to digging pressure). *Coptotermes formosanus* (Rule 9)

- Biomechanics for small particles include 1) anchoring 2) compression and 3) transport (considered formation i.e. pellet formation). *Soloenopsis invicta* (Rule 13)

Excavation rule 2 was implemented by having the robot sense which direction the granular media was using a low, forward-facing IR sensor. This sensor would identify the robot's proximity to the granular media during the roaming phase, and would also identify the robot's proximity to the depository area during deposition. Rule 4 was implemented using a laser sensor that would give a binary output for whether or not the robot was in queue behind another robot near the excavation face. The digging steps would start with the robot approaching the granular media, then stopping before the excavation face and then checking for a queue before finally approaching the face to dig. Rule 6 was implemented by making sure that the robot was outside of the arena before dropping off the excavated material. In order to employ rule 9, the robot was to make decisions using only information gathered about the arena from external sensors. Finally, biomechanics for small particles were used because the robot was designed to excavate in a loose, flowable granular media.



Figure 6.1: Sloped experimental test bed filled with granular media for excavation.

Chapter 7

GRANULAR MEDIA CHARACTERIZATION

If excavation is to occur, a large quantity of granular media will be needed. Considerations that were taken during the selection process were whether or the the granular media will damage the robot, whether or not the shape of the granular media was uniform, and if the motors available would be able to overcome the surface forces of the granular media to initiate excavation. Detailed in this chapter are the theory and methods for determining if the chosen granular media was right for the experiment.

7.1 Granular Media Selection Process

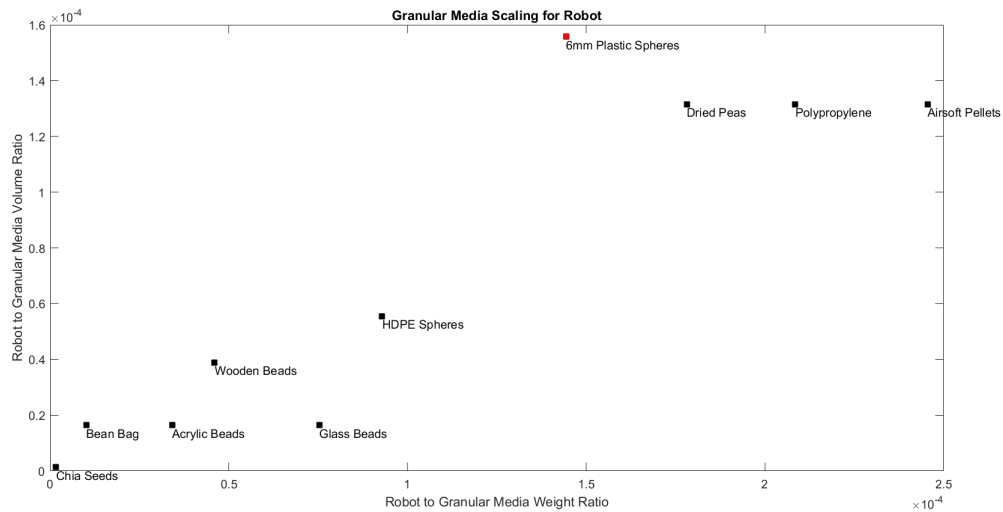


Figure 7.1: Examples of different spherical granular medias and their robot weight/volume ratio.

The process by which the final granular media for experiments was selected used

comparisons between studies involving other robots that were able to successfully navigate through a given media. The specific study used was for a sand-swimming robot from the CRAB Lab at GATech, where their robot used a bed of 6mm plastic spheres to swim through using sine wave motions [Maladen *et al.* (2011)]. A comparison was done where the volume ratios between the robot and individual granular media were plotted against the weight ratios between the robot and granular media, and can be seen below in figure [FIG] After plotting various examples of uniformly spherical granular media, it seemed that the media with the closest ratios to those used in Maladen *et al.* (2011) were dried peas. Dried peas also presented another advantage to this thesis for being both low-cost, easily accessible and biodegradable.



Figure 7.2: Dried peas were ultimately selected for excavation materials due to their low cost, low density and uniformly spherical shape.

Initially, a terradynamic analysis was to be done on the granular media to use force fitting functions to characterize the resistive forces during excavation. Unfortunately, the assumptions used in order to use terradynamics limited the sphere size from 0.1-1mm, and the average sphere size of dried peas was measured to be approximately 5mm. For that reason, the following force experiment was designed.

7.2 Force Experiments

The test bed for the experiment was built out of 3D printed parts, a resistive force sensor, a plastic tub and an Arduino Uno. It was then filled with dried peas and fit with a motor and whег design.

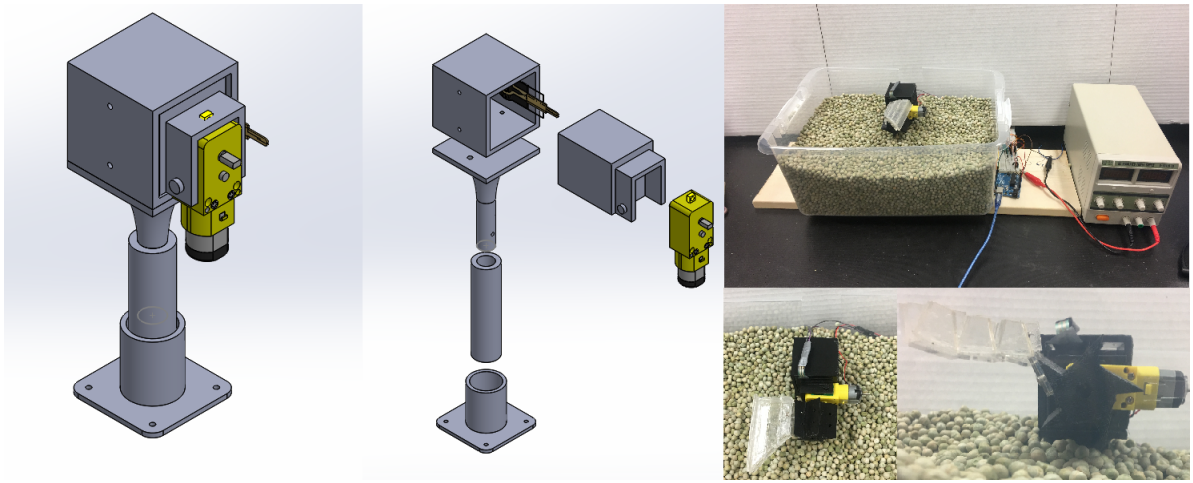


Figure 7.3: (1) Solidworks models for test stand holding motor and resistive force sensor. (2) Actual test bed setup using wheel bracket, whег design, power supply and Arduino Uno.

The test bed works using a 3D printed cube fitted with a motor and placed inside of a bracket. The bracket itself has a resistive force sensor, and is adjustable to be rotated based off of what direction the desired measurements are in. The fitting between the cube and the bracket is just loose enough to acquire accurate

measurements as the motor transfers its forces during digging. The experiment was done with the resistive force sensor in the horizontal and vertical positions if looking at the setup head on. The vertical measurement was considered the F_y direction, while the horizontal measurement was considered the F_x direction.

Resistive force sensors are notorious for their roughly 25% error margin, however this was deemed passable for design purposes. In order to make sense of the data taken, ten trials were run for the F_x and F_y directions. Each trial was fitted with a fifth-order approximation, and those fifth-order approximations were fitted again to give a final function. Then, the local extrema were used to determine the maximum forces that occur during a cycle. It was noted that the experimental setup was already exerting forces on the sensor before the rotation began, so that value was subtracted from the functions before calculating the extrema. After using the manufacturer's log-log resistance to gram conversion chart, the final maximum forces were calculated to be 18 grams for F_x and 27 grams for F_y . Plotted below in Figure 6.3 are the fitted functions from the trials in the F_x and F_y experiments, along with a plot of the two forces simultaneously where the forces exerted by the test bracket were removed.

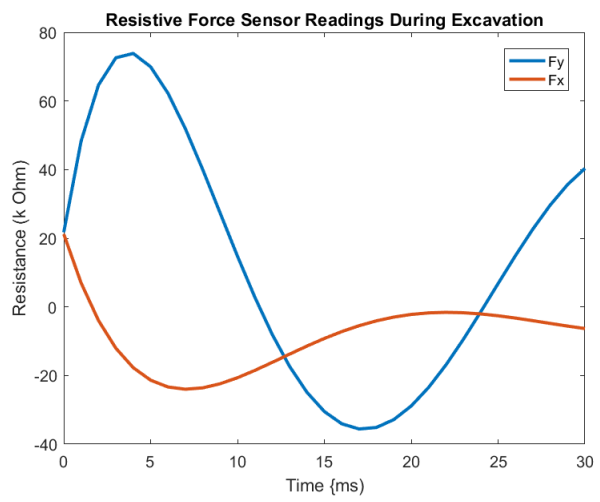
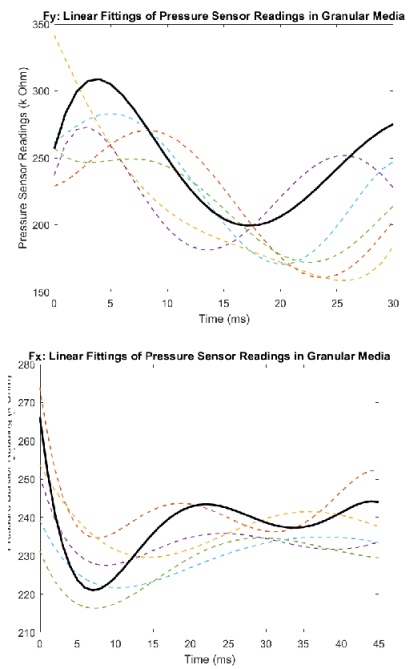


Figure 7.4: .

Chapter 8

ROBOTIC PLATFORM

The second component of the experimental test bed is the excavating robotic platform. The design for the chassis and whogs were developed from bio-inspired and foldable robotics to create a final low-cost excavating prototype. Ultimately three different prototypes were built, each with a new design strategy informed by the prototype before it. With a process as complex as excavation, early failures were necessary and guiding factors to the final prototype.

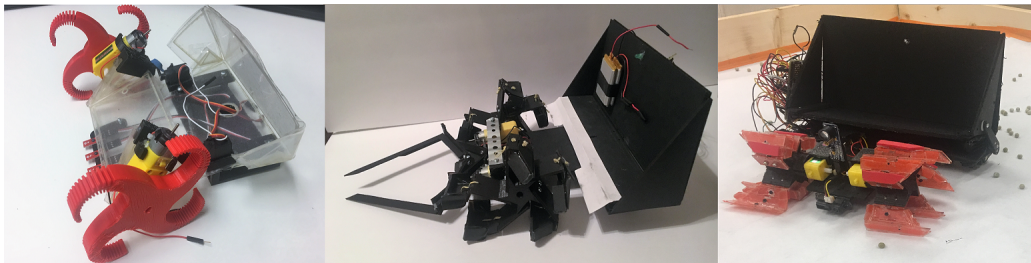


Figure 8.1: (1) The very first acrylic prototype, featuring an IR sensor and 3D printed whogs with a foldable chassis (2) The second posterboard prototype, with stabilizing mandibles, forward facing IR sensor, actively sensing media carriage and foldable whogs (3) Final acrylic and fabric prototype, featuring a suspension system, dumping mechanism, actively sensing media carriage, foldable whogs and two IR sensors

The inspiration for the design began with a simple concept: the robot was to locomote and excavate using just the motors on the wheels, and no additional mechanisms were to be used for excavation. Initially the chassis itself was to fold to change the angle of attack for the wheels, however after considering the success of modern

dredge mechanisms a folding wheel-leg (whieg) mechanism was adapted. In order to achieve excavation and locomotion with the same design, the motors would rotate in the forward direction which would pull the whiegs in using angular momentum and create a nearly circular wheel for forward motion. Then, when the motors rotated in the opposite direction the whiegs would be pulled out and effectively scoop up granular media during each rotation, similar to dredge mechanisms.

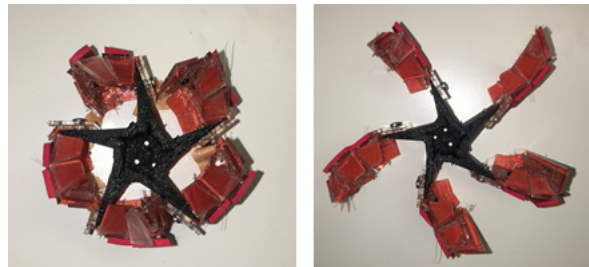





Figure 8.2: Final excavating and locomoting mechanism

8.1 Experimental Goals

The goal of the experiment is to verify that the prototype is capable of the roaming, excavating and depositing phases defined in the algorithm. Once capable of these phases, the robot is to be equipped with the proper sensors to recognize if it is behind another robot or at the excavation face. In the instance of a queue, robot will be able to wait for a period of time and then turn to expand the structure to continue excavation. Given these few capabilities, it is assumed that the robot would be able to execute the algorithm designed and simulated earlier.

The sensors chosen for the final robotic platform were an IR sensor, a laser sensor and a force sensor. The IR sensor is located low and in front of the robot chassis, and actively measures the distance between the robot and the granular media. Once the robot is traversing the pit of granular media, the sensor will begin to read the robot's close proximity which will initiate excavation. Immediately before excavation, the

laser sensor will read directly in front of the robot and use a digital reading of either 0 or 1 to see if it is in a queue. If not, the robot will dig at the excavation face. If it is in a queue, the robot will wait for the CWP and then check to see if it is still behind another robot. If the robot is still in line, it will turn and initiate excavation at a new excavation face. During excavation the force sensor on the platform will tell the robot when the collection bin is full, and this will be the signal to begin the deposition cycle of the experiment. The robot will rotate one motor until the IR sensor reads the otehr end of the test bed, and then drive to deposit. This will complete a single excavation cycle.

Photo	Part	Use
	0.5" Circular Force Sensing Resistor	Collection Bin Sensing
	Sharp Analog Distance Sensor	Ground and Granular Media Detection
	Obstacle Detection Sensor	Obstacle Detection

8.2 Overview of Foldable Robotics

Inspiration strikes at unpredictable moments, and interest in pursuing an origami-inspired robot for this thesis started after a printing accident left 200 unusable sheets of paper in the hands of one guilty graduate student. The benefits of foldable robotics include their simplification of complex mechanisms into one small mass prototype,

their fast manufacturability, and their low cost. By strategically planning the locations of folds, foldable robots can get multiple degrees of freedom from one part that would normally require several off-the-shelf parts. In the beginning of the prototype design several different paper and cardboard prototypes were built, but paper building materials were eventually abandoned for active parts and the final design was made of acrylic sheets with flexible fabric layers, an illustration board chassis and 3D printed brackets.

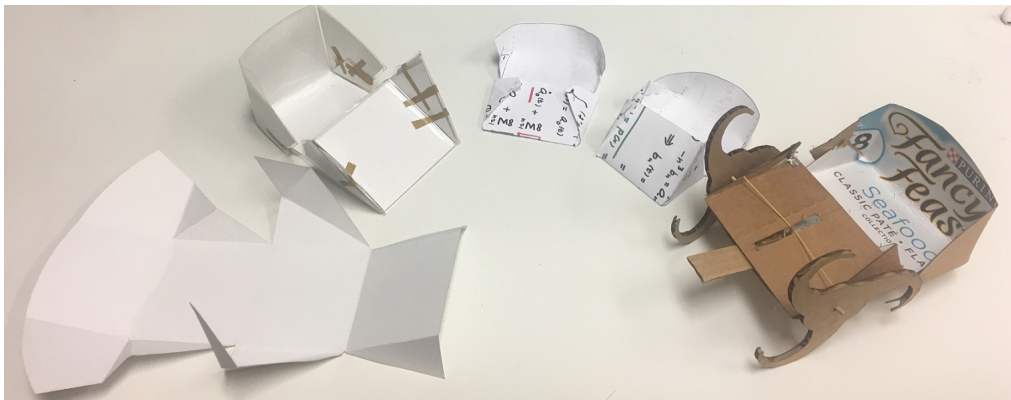


Figure 8.3: Initial origami chassis ideas, made of scrap paper and cardboard

Foldable robotics first started as a manufacturing method for micro hinges back in 1992, using Polysilicon structures on a micro level to form complex 3D designs on a small scale Pister *et al.* (1992). Future designs were actuated using piezoelectric sensors Hoover and Fearing (2008), until the mechanisms began to be used in larger scale designs. Common actuators were eventually added to the equation, which gave way for many of the foldable robotic designs seen in research today. As foldable mechanisms gained popularity and began to be more widely used, in 2017 DASH Robotics, Inc. collaborated with Mattel, Inc to commercially sell their foldable Kamigami robot as a children's toy Humphries (2017).

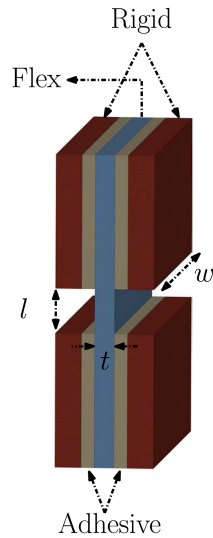


Figure 8.4: Example of a 5 layer foldable hinge

Laminate manufacturing methods are unique to the construction of foldable robotics. The concept is to strategically cut out the mechanisms internal details per individual layer, then align each of the robots layers and adhere them together. Once adhered, the final outline of the part is cut and it is finally free to fold and flex into shape. The final robot design in this thesis uses five layers to create one sheet of building material that contains joints, holes, and a flexible layer for the robots mechanisms. The first layer of the design is of the robots outer chassis material, the second layer is an adhesive layer, the third layer is the flexible layer, the fourth layer is another adhesive layer, and the fifth layer is another layer of the material.

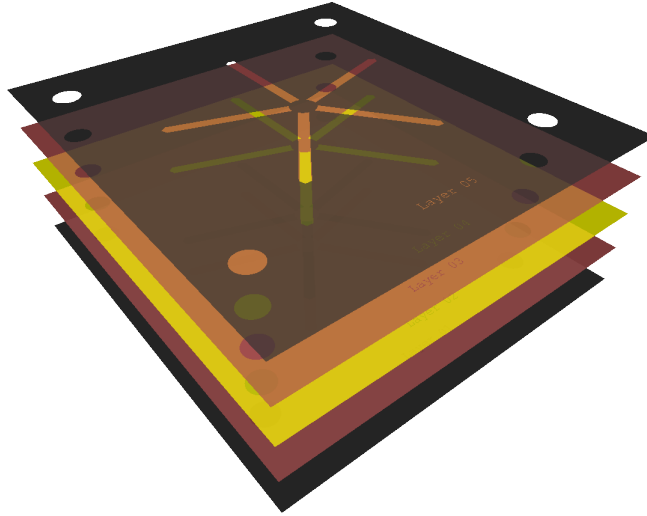


Figure 8.5: Example of the five layers before being adhered and cut out

8.3 Motor Selection

The kinematics of an individual spoke on the whег mechanism were modeled using a script in Python to understand what kind of motor would be necessary to overcome the forces experienced during excavation. Initial designs were simple two link mechanisms, for which the following Free Body Diagram was generated:

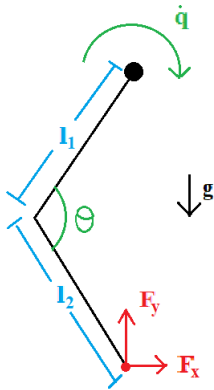


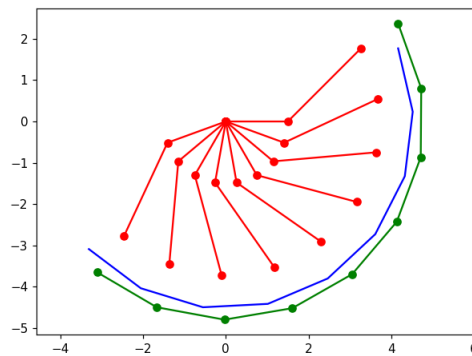
Figure 8.6: Free Body Diagram for a two-linked whег mechanism as it rotates through granular media

Where the variables in Figure [FIG NUMBER] were:

$$\begin{bmatrix} l_1 \\ l_2 \\ \theta \\ F_x \\ F_y \\ q \end{bmatrix} = \begin{bmatrix} 1.5'' \\ 2.5'' \\ 135 \text{ deg} \\ 0.177 \text{ N} \\ 0.265 \text{ N} \\ 0 - 180 \text{ deg} \end{bmatrix}$$

The Python script was then used to generate the following trajectory for the two-link whег spoke design as it excavates through the media:

Figure 8.7: Whег trajectory plot from Python script



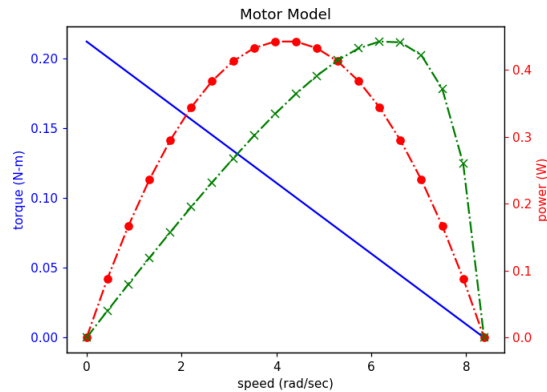
This trajectory was then to generate a Jacobian for the system, and the range of motion at the input was compared to the range of motion at the output to identify the relationship between motor speed and force via the following relationships:

$$\tau = J^T \begin{bmatrix} F_x \\ F_y \end{bmatrix}$$

$$P = J\omega$$

After a desired output speed was chosen, several different motor specifications were used in the code to choose the final a DC motor with the following motor efficiency curve:

Figure 8.8: Motor Torque-Speed-Efficiency Curve



8.4 Mechanism Design Evolution



Figure 8.9: The locomoting (left) and excavating (right) modes of the first prototype

The first prototype designed (pictured in Figure [FIG]) consisted of a chassis made out of laser cut acrylic compressed between two sheets of laminating plastic. Since this chassis had of two flexible layers sandwiching a rigid layer, the design would often seize up while it moved as pressure built up in the outer layers of the design. This prototype incorporated 3D printed whegs, and the chassis itself was to fold

to change the angle of attack of the whigs to initiate excavation. Underneath the robot were three IR sensors meant to execute a line follower algorithm to simulate a pheromone trail that would lead into the granular media, and the folding mechanism was actuated by two servos. This robot was critically actuated, using two motors and the two servos to move. Unfortunately, the combination of differential drive and rigid whigs resulted in such a bumpy driving pattern that the IR sensors were rendered useless, and other sensing and driving methods were investigated.

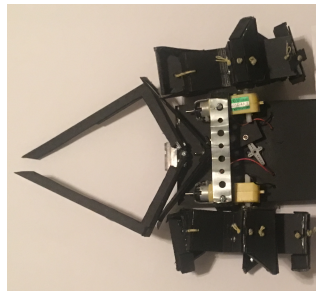


Figure 8.10: Stabilizing mandible mechanism made completely out of laminate parts

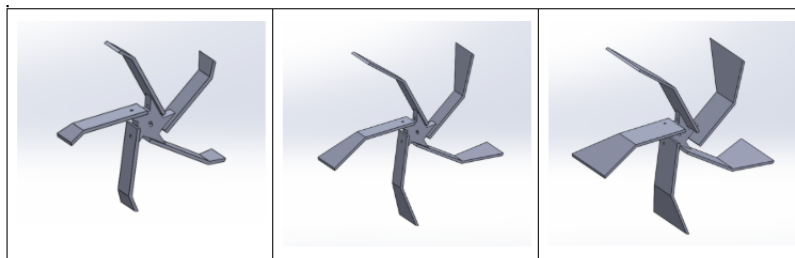


Figure 8.11: Examples of different foldable whigs attached to wheel brackets.

The second prototype used the concepts central to foldable robotics, where the chassis, whigs and mandible consisted of 5 layer laminate manufactured parts. This designs sensing abilities included a resistive force sensor underneath the carrier portion of the chassis, alongside an IR sensor in front of the chassis. The main idea was that the robot would locomote up to the pit of dried peas and sense a stabilizing beam

placed in the pit. The mandibles would grab onto the stabilizing beam and use it to prevent forward and backward motions as the motors started excavation. Then, when the resistive force sensor sensed that the carrier chassis was full, it would turn the motors off. This design proved to be an efficient excavator, however did not offer any solutions on how to get the granular media out of the chassis after excavation was complete. The most successful part of this prototype were the foldable whegs, which accomplished the design goal of locomoting in the forward direction while excavating in the backward direction. It was observed after the prototypes completion that the weight of the robot was sufficient to hold the whegs in place during excavation, so the mandible design was scrapped and the servo used for them was repurposed to solve the issue of depositing.

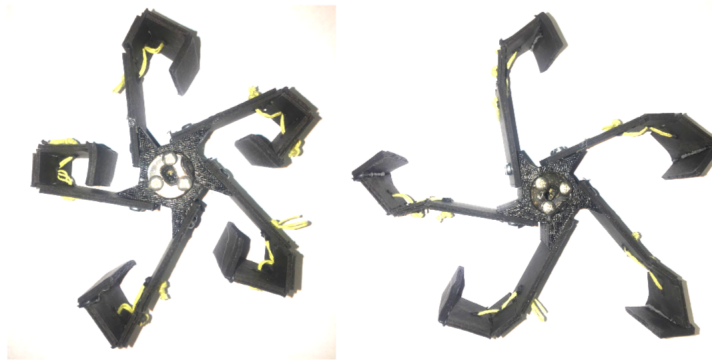


Figure 8.12: Cardboard foldable wheg design from second prototype in locomoting (left) and excavating (right) modes.

Since the second prototype was made out of cardboard, the whegs were more susceptible to damage during their rotations through the granular media. After enough trials, the cardboard pieces eventually de-laminated or the thin plastic flex layer tore through the hinges, leaving most of the whegs beyond repair after enough trials. This left room for improvement in the wheg materials as well as the their flexible layer.

Furthermore, the whogs themselves would still bounce during locomotion to the extent that forward motion was uncontrollable. This was due to the rigid and angular nature of the whogs, and it was established that future whogs would need some kind of curvature to allow forward locomotion.



Figure 8.13: Final acrylic whogs with reinforcing fabric flex layer. Locomoting mode (center) and excavating mode (right). Rotations are limited by the whog material thickness during excavation.

For the next iteration of whogs, an extra link was added and adhered in a curved position so that when the motors ran forward the compressed whogs would appear nearly circular. Cardboard was traded for thick acrylic, and the thin plastic flex layer was traded for a sturdy fabric layer. These two changes increased the durability of the whogs to the extent that they could endure excavation cycles with no signs of breaking.

Finally, the servo that had been added to the design for the mandibles was repurposed as a lever arm to dump the chassis during the deposition cycle, and can be seen below in Figure 7.11.

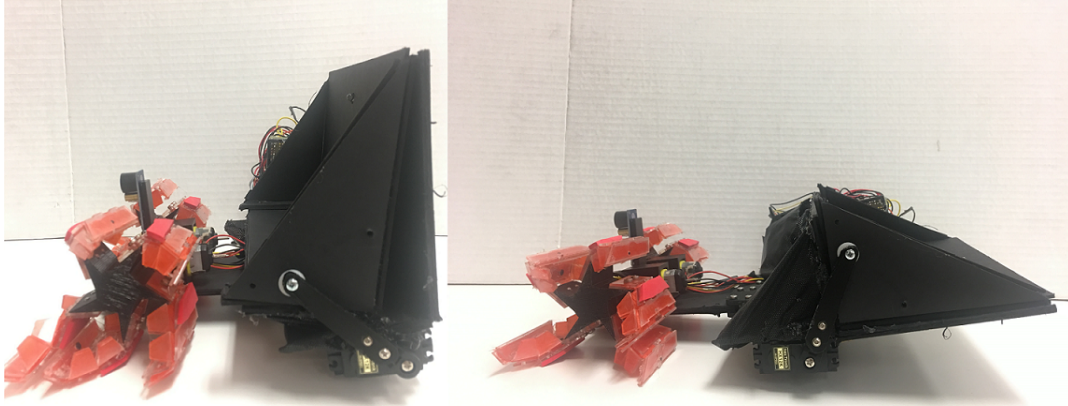


Figure 8.14: Servo-actuated dumping mechanism from final design

8.5 Final Design

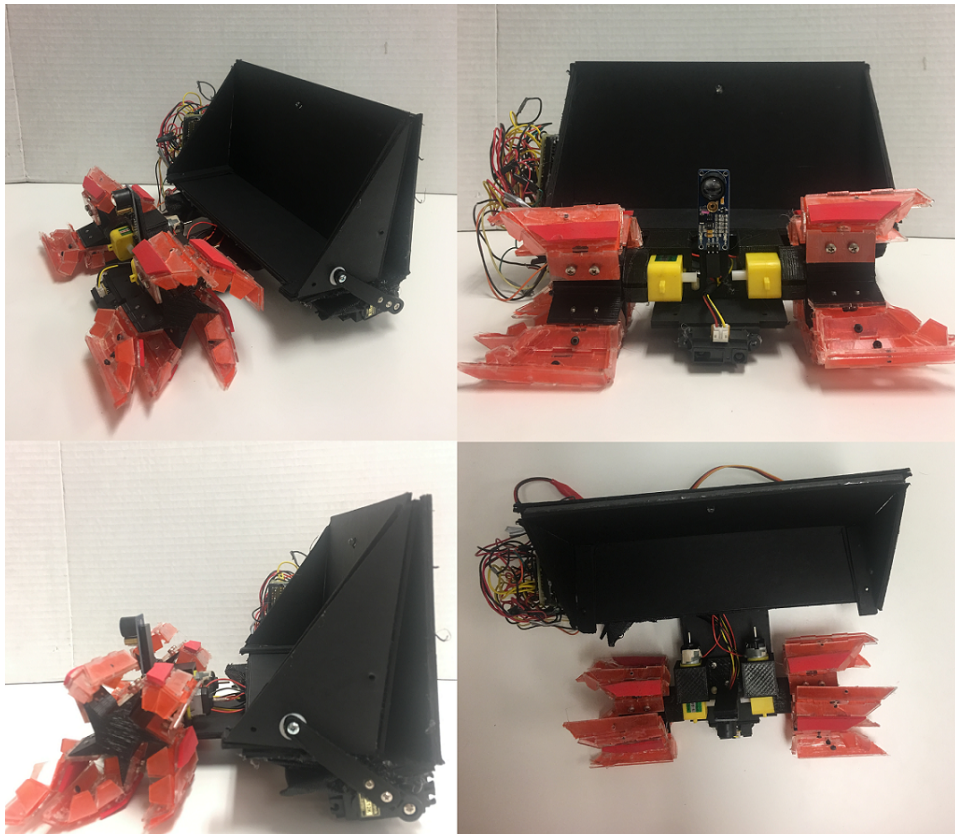


Figure 8.15: Final robot design

The final design ultimately wound up being a hybrid material design, with a cardboard chassis and plastic whogs. The servo was upgraded from a microservo to a standard servo to offset the force of the dried peas filling the chassis, the resistive force sensor was kept underneath the chassis carrier, and a laser sensor was added to determine if the robot was behind an object (or in queue).

8.6 Manufacturing Process and Part Files

The chassis was cut from illustration board and manufactured according to standard foldable robotics procedures. The whogs were cut from acrylic and manufactured normally, however in order to reinforce the curve of the whogs the acrylic was placed in a mold that would hold up the folding edges to form a scoop. The edges were held rigidly while the only folding part of the mechanism was the part of the whog that swung either open or closed. Pictured below in Figure 7.13 are the cut files for the first layer of material, the flexible layer, the second layer of material, and the final cut for all 10 whogs in the design. The rest of the robot brackets and lever arms were made from 3D printed ABS plastic and secured using M3 screws.

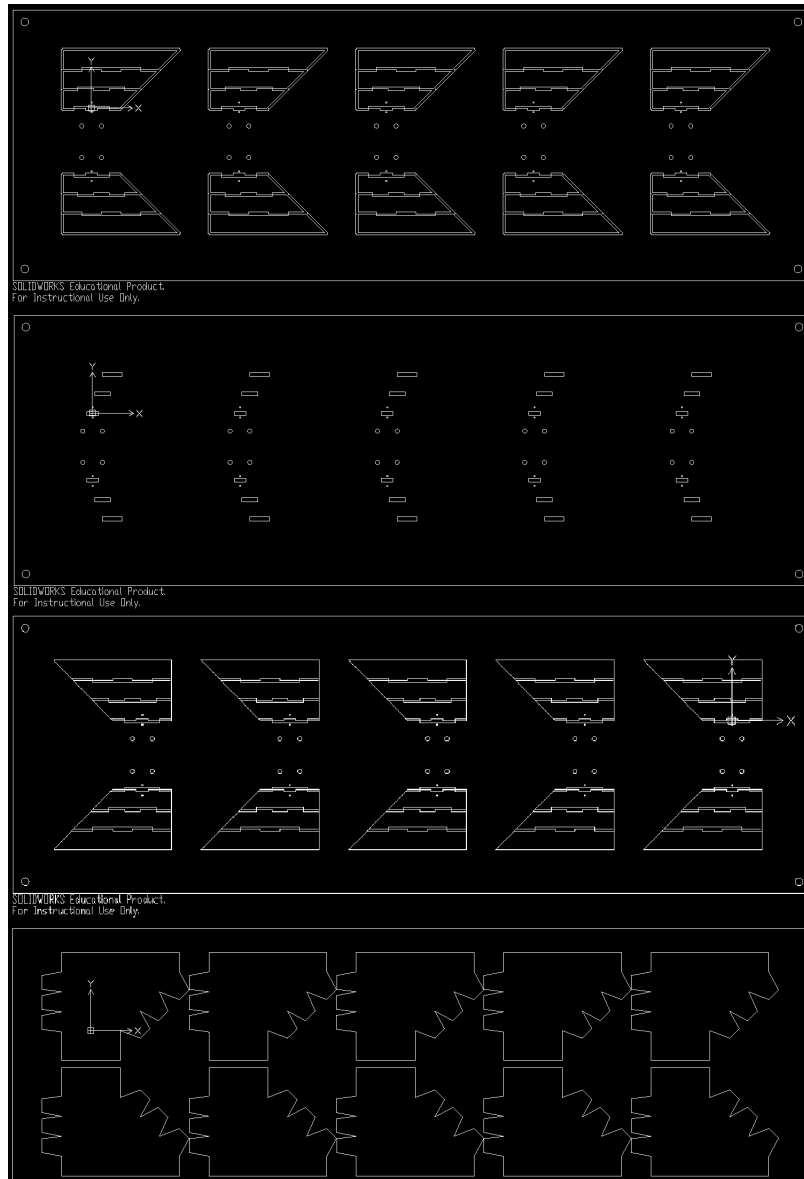


Figure 8.16: Cut DXF files for final set of 10 whegs.

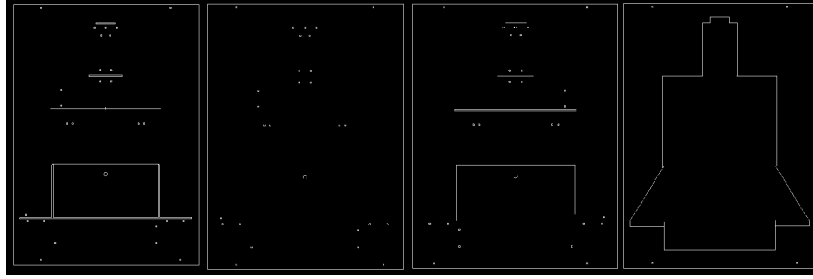


Figure 8.17: Cut DXF files for final chassis

8.7 Code Logic

The code was written in Arduino and uploaded to a Pro Trinket for execution. The code itself was structured like the NetLogo simulation, however it used different visual cues through the IR sensors. The first step of the code would read the IR sensor value, and if it was under what was needed for the granular media the motors would drive forward and into the granular media until the designated value was reached (signifying the excavation face). Then, the robot would use its laser sensor above the chassis to get a reading of either 1 or 0 for whether or not the robot was in queue. If the sensor read 1, then the robot would begin its critical waiting period. If the sensor read 0, it would begin excavation. After the CWP passes, the robot checks again to see if it is still in queue. If not, it begins excavation. If the robot is still in queue, it will turn and initiate a new excavation face. During excavation, the resistive force sensor is reading the amount of dried peas filling up the chassis. When the desired amount is reached, the robot will stop excavating and turn to face the opposite end of the arena. Then the robot will begin deposition by locomoting to the opposite end of the arena until a desired IR sensor value, and then activate the servo to dump the chassis away from the pit.

Chapter 9

EXPERIMENTAL RESULTS



Figure 9.1: The robot in position for (1) Roaming (2) Excavating (3) Depositing

Ultimately, the final robot design was capable of executing the cycles of roaming, excavation and deposition independently, however the robot was unable to complete each cycle back-to-back. One of the biggest challenges to robotics is the ability to navigate across changing surfaces, and unfortunately the robot design was unable to drive from a flat surface onto one filled with granular media. This feat has been successfully achieved with other whegged robots (such as the RHex models [Saranli *et al.* (2001)]), however the final whieg design was so rounded in the locomotion phase that it behaved exactly like a wheel in the forward direction. This resulted in the robot getting stuck every time it reached the granular media. Different test bed approaches were used to hopefully aid with the transition, but results did not show any improvements using a sloped, unsloped, smooth or frictional test bed.

9.1 Locomotion

The robot was able to successfully use the folding whieg design to move forward. Slipping became an issue while in motion, so strips of gripping tape were added to

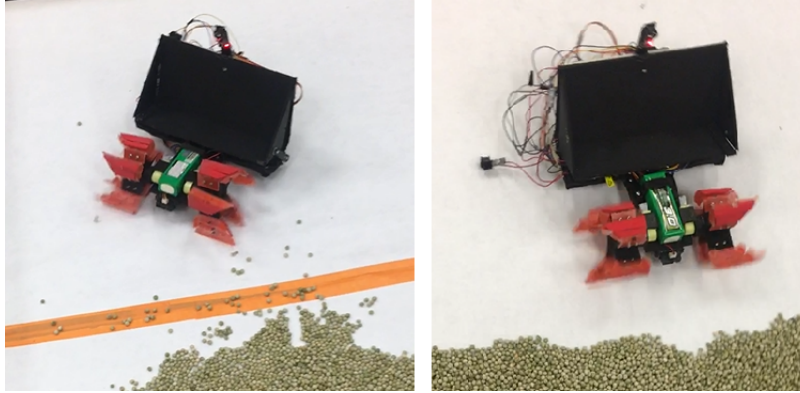


Figure 9.2: Different headings of robot during locomotion

the side of the wheel in contact with the ground. This improved the robot's forward motion significantly. In regards to directional control, the robot was able to sense and move forward when the IR sensor that reads the granular media is under a certain value. Unfortunately, the presence of the IR sensor did not guarantee directionality control, and the robot had a tendency to stray to the right of the arena. This could be accredited to a weight imbalance somewhere within the system. Regardless, the robot still made it up to the edge of the granular media successfully with the current wheel design.

9.2 Transition

The main issue preventing the robot from completing an excavation cycle was its inability to make the transition from solid ground to a ground covered in granular media. Different factors contributed to this, one being the wheel shape as it moves into the granular media and another being the friction from the back of the carrier chassis. Once the robot reached the granular media, the wheels would simply spin over the loose media and motion was stopped.

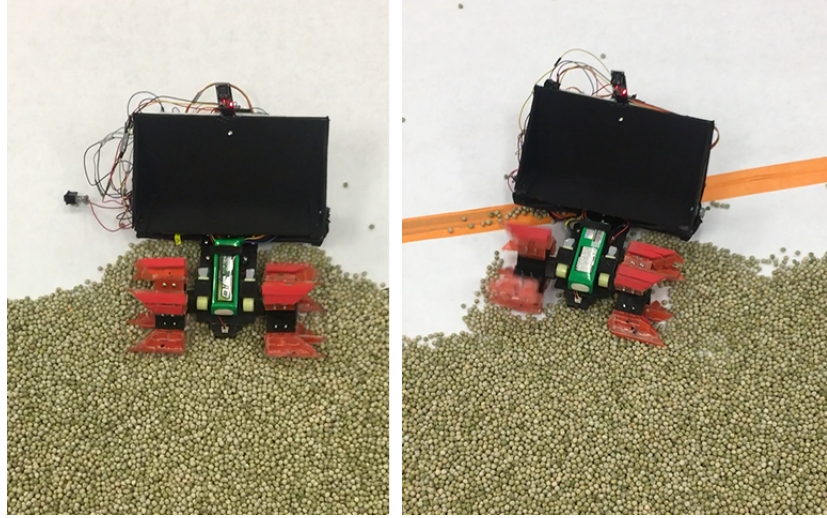


Figure 9.3: Examples of robot stuck on edge of granular media

9.3 Excavation

Despite stopping at the edge of the granular media, if the robot was placed into the deeper end of the arena (where the media reached a depth of about 3 inches), the design was able to successfully excavate. When the IR sensors sensed a proper depth, the robot knew to check the laser sensor for a queue, then either wait or run the motors backwards while the resistive force sensor would detect how much media was filling the carrier chassis. Once a full chassis was detected, the motors would stop and a signal would be sent to the LED to light up. From here, the robot would turn around and begin deposition. Unfortunately, due to the same reasons the robot couldn't transition into the media, the robot was incapable of turning around in the granular media after excavation using the present whleg design.

9.4 Deposition

If placed outside of the granular media, the robot was able to move away from the granular media to a distance that would allow the robot to deposit. Once the

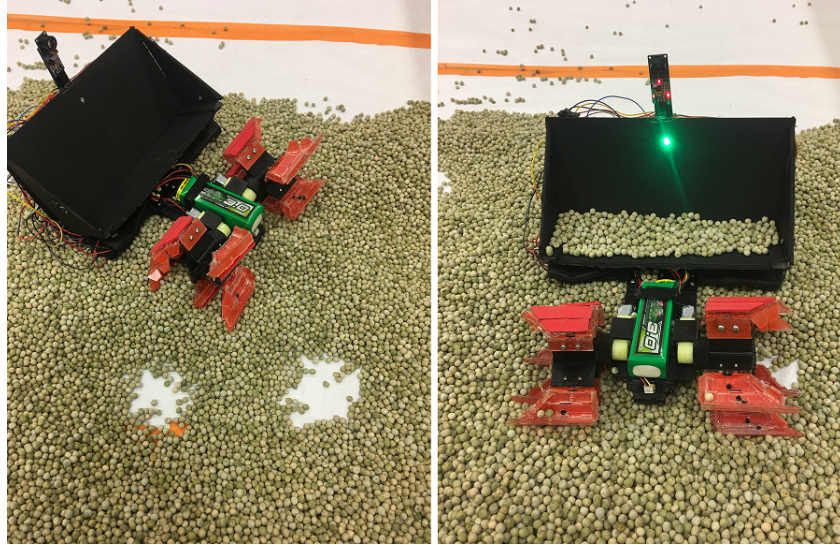


Figure 9.4: Excavation patterns left by robot and LED activation with full chassis

IR sensor sensed the opposite end of the arena, the servomotor received a signal to rotate and deposit the contents of the carrier chassis. Then, the robot would drive away while the media fell out of the flattened chassis.

9.5 Discussion

During the experiment, de-lamination of the foldable parts remained a consistent issue as the whogs rotated about the motor. When this occurred, the de-laminated parts were glued back into place, resulting in a stronger reinforced material. Thankfully, the final configuration of fabric and acrylic never broke beyond de-lamination, which was an improvement from the old illustration board and polyester prototype. The design was also successful at locomotion up to the granular media using information from the IR sensor, and was able to detect the presence of a full chassis of dried peas after excavation from the resistive force sensor. It was also able to check to see if it was in queue after arriving to the excavation face using digital readings of 1 or 0 from the laser sensor. Unfortunately the robot was unable to turn and begin

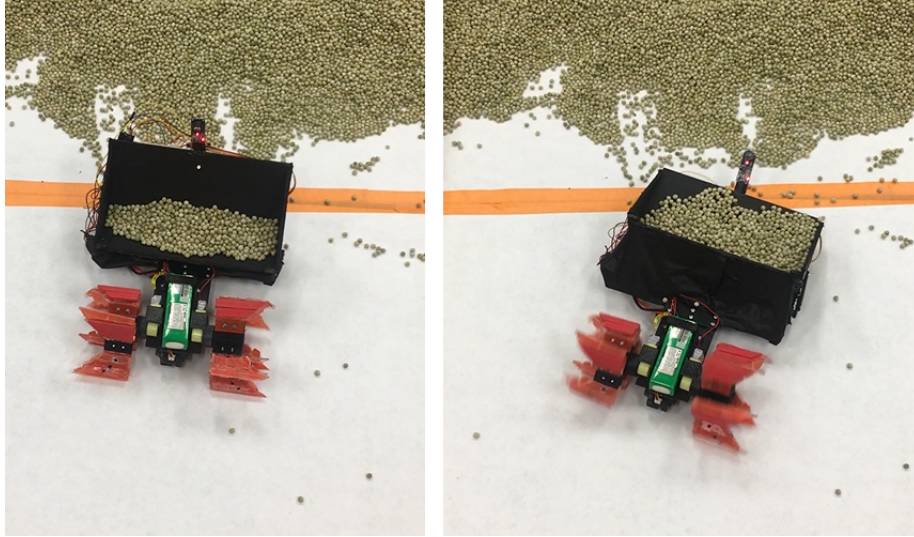


Figure 9.5: Robot depositing outside of arena

the tunnel widening portion of the algorithm due to its inability to traverse over the granular media.

In evaluating the efficiency during excavation, it was noted that the motors were programmed to move the foldable whegs through the granular media only at high speeds. This resulted in some of the media becoming airborne and lost, which had a negative effect on the amount of time it took to excavate a full chassis of media. Attempts were made to excavate at slower speeds using smaller voltages, however the success of excavation was dependent on the motor speed due to the chassis design. Lower speeds resulted in the media being gently carried for a complete cycle and then dropped back onto the ground, never becoming airborne enough to land in the back of the carrier chassis. Regardless of the media lost at high speeds, the system was still effective at consistently excavating a full chassis.

By using the non-dimensional metrics to evaluate efficiency defined in section 3.3, the efficiency of the robot is compared to the efficiency of the *Formica pallidefulva* ant in the following table:

Excavator	Power Ratio	Mass Ratio	Final Efficiency Score
Ant (<i>Formica pallide-fulva</i> & <i>Solenopsis Invicta</i>)	0.2000 [Tschinkel (2006)]	0.3000 [Tschinkel (2006)]	0.6667
Foldable Robotic Excavator	0.0400*	0.2100	0.1900

**Note that robot was unable to transition into granular media, therefore the energy consumption did not take into account the power required to reach the excavation face.*

Evaluating the robot design overall, the robot was successful at locomotion, excavation and deposition. The sensors were capable of making decisions that were explicitly defined in the algorithm, where the IR sensor would draw the robot to the media, the laser sensor would identify if the robot was in queue, and the carrier chassis would identify if the robot was loaded and could initiate deposition. Despite the issues experienced at the entrance of the granular media test bed, the design was successful at all other aspects mentioned in the algorithm.

CONCLUSION AND FUTURE RESEARCH

10.1 Conclusion

The ideas presented in this thesis lay the groundwork for a new perspective on bio-inspired swarm excavation. After three prototypes, the final design was able to execute the three algorithm phases independently, however completing all three cycles back to back was not possible with the current whег design. In simulations, the simple algorithm was able to successfully control the tunnel shaping of the final arena regardless of population size. Then, the data collected from the simulation was able to produce a model that could predict a waiting period based off of a population size and a desired tunnel shape. Connecting the simulations to the experiment, the robot itself was able to complete each of the phases defined in the simulation (roaming, excavating and depositing), while picking up queues from information gathered from the sensors. Unfortunately, the final whег design was unable to traverse over the granular media, resulting in the robot being unable to complete all of the cycles back-to-back.

The results indicate that the simulation model can be used to design controllers for robotic excavation for tunnels in construction, or large cavities in the case of a search and rescue operation. By controlling the behaviors of individual agents with a time delay (i.e. the CWP), it is possible to control the architecture of the final structure.

10.2 Future Goals

Future goals will be to include ways to explore different factors of excavation such as varying the excavated materials, creating branching patterns, or increasing the depository distances. The purpose of the algorithm design is to eventually implement the CWP alongside a swarm of the robotic platform to have collective excavation.

From a design perspective, laminate manufacturing may be adjusted to include stronger adhesives to prevent the issues experienced with de-lamination during excavation. In order to tackle the problems experienced with transitioning into the pit of dried peas, a new foldable whег design could be developed that would maintain a whег shape in the forward direction during locomotion. In order to successfully combine differential drive and whегs, a suspension system would need to be developed so that the bouncing nature of the whегs would not compromise IR sensor readings. To make transporting the carrier chassis easier, the carrier portion of the chassis could be moved closer to the the center of gravity of the robot to ease the strain on the motors from dragging a full chassis behind it. Future implications of the robot itself could abandon the media carrier entirely and initiate the robot in self burial in a loose granular media (which has applications in security operations or agriculture). Finally, by incorporating other elements of excavation (such as digging efficiency, power consumption, or excavating material density), a more realistic approach to bio-inspired swarm excavation can be designed. By embracing the intricate details of the system, autonomous collective excavation is brought one step closer to implementation in construction, search and rescue operations, or extraterrestrial exploration.

REFERENCES

- “The boring company, faq”, <https://www.boringcompany.com/faq/>, accessed: 2018-7-7 (2017).
- “Accident search results, osha.gov”, <https://www.osha.gov/pls/imis/AccidentSearch>, accessed: 2018-7-7 (2018).
- “How do ants behave in an ant farm?”, <http://antfarmsforkids.com/how-do-ants-behave-in-an-ant-farm>, accessed: 2018-7-16 (2018).
- “Nasa’s ninth annual robotic mining competition rules and rubrics”, https://www.nasa.gov/sites/default/files/atoms/files/2018_rulesrubrics_partii.pdf, brochure (2018).
- “West michigan site preparation & excavation”, <http://www.milbocker.com/site-preparation-excavation>, accessed: 2018-7-16 (2018).
- Bardunias, P. and N.-Y. Su, “Opposing headings of excavating and depositing termites facilitate branch formation in the formosan subterranean termite”, *Animal Behaviour* **78**, 3, 755–759 (2009).
- Bardunias, P. M. and N.-Y. Su, “Queue size determines the width of tunnels in the formosan subterranean termite (isoptera: Rhinotermitidae)”, *Journal of insect behavior* **23**, 3, 189–204 (2010).
- Burd, M., N. Shiwakoti, M. Sarvi and G. Rose, “Nest architecture and traffic flow: large potential effects from small structural features”, *Ecological Entomology* **35**, 4, 464–468 (2010).
- Camazine, S., J.-L. Deneubourg, N. R. Franks, J. Sneyd, E. Bonabeau and G. Theraula, *Self-organization in biological systems*, vol. 7 (Princeton university press, 2003).
- Espinoza, D. N. and J. C. Santamarina, “Ant tunneling in granular media perspective”, *Granular Matter* **12**, 6, 607–616 (2010).
- Gravish, N., M. Garcia, N. Mazouchova, L. Levy, P. B. Umbanhowar, M. A. Goodman and D. I. Goldman, “Effects of worker size on the dynamics of fire ant tunnel construction”, *Journal of The Royal Society Interface* p. rsif20120423 (2012).
- Hoover, A. M. and R. S. Fearing, “Fast scale prototyping for folded millirobots”, in “Robotics and Automation, 2008. ICRA 2008. IEEE International Conference on”, pp. 886–892 (Ieee, 2008).
- Humphries, M., “Mattel launches kamigami build and code robots for kids”, URL <https://www.pcmag.com/news/356722/mattel-launches-kamigami-build-and-code-robots-for-kids>, [Online; posted 11-October-2017] (2017).

- Iai, S., *Geotechnics and earthquake geotechnics towards global sustainability*, vol. 15 (Springer Science & Business Media, 2011).
- Linevich, V., D. Monaenkova and D. I. Goldman, “Robophysical study of excavation in confined environments”, *Artificial Life and Robotics* **21**, 4, 460–465 (2016).
- Lislerud, A., “Hard rock tunnel boring: prognosis and costs”, *Tunnelling and Underground Space Technology* **3**, 1, 9–17 (1988).
- Maladen, R. D., Y. Ding, P. B. Umbanhowar, A. Kamor and D. I. Goldman, “Biophysically inspired development of a sand-swimming robot”, (Georgia Institute of Technology, 2011).
- Petersen, K., R. Nagpal and J. Werfel, “Termes: An autonomous robotic system for three-dimensional collective construction”, *Proc. Robotics: Science & Systems VII* (2011).
- Pister, K. S., M. Judy, S. Burgett and R. S. Fearing, “Microfabricated hinges”, *Sensors and Actuators A: Physical* **33**, 3, 249–256 (1992).
- Pratt, S., personal communication (2017).
- Rosenthal, B. M., “The most expensive mile of subway track on earth”, *New York Times* (2017).
- Saranli, U., M. Buehler and D. E. Koditschek, “Rhex: A simple and highly mobile hexapod robot”, *The International Journal of Robotics Research* **20**, 7, 616–631 (2001).
- Siciliano, B. and O. Khatib, *Springer handbook of robotics* (Springer Science & Business Media, 2008).
- Thangavelautham, J., K. Law, T. Fu, N. A. El Samid, A. D. Smith and G. M. D’Eleuterio, “Autonomous multirobot excavation for lunar applications”, *Robotica* **35**, 12, 2330–2362 (2017).
- Tschinkel, W. R., “The nest architecture of the florida harvester ant, *pogonomyrmex badius*”, *Journal of Insect Science* **4**, 1 (2004).
- Tschinkel, W. R., *The fire ants* (Harvard University Press, 2006).
- Wilensky, U. and W. Rand, *An introduction to agent-based modeling: modeling natural, social, and engineered complex systems with NetLogo* (MIT Press, 2015).

APPENDIX A

NETLOGO CODE

```
globals [  
  soil  
  branches]  
  
patches-own [  
  GAV  
  deposit  
  deposit?]  
  
turtles-own [  
  excavate  
  roam]  
  
to setup  
  clear-all  
  setup-turtles  
  setup-patches  
  exc-face  
  reset-ticks  
end  
  
to setup-patches  
  ask patches  
  [ setup-GAV ]  
  setup-soil  
end  
  
to setup-GAV  
  set deposit? (distancexy -10 -10) < 2  
  if pycor <= 16 and pycor >= 14  
  [set GAV 16]  
  if pycor < 14 and pycor >= 12  
  [set GAV 15]  
  if pycor < 12 and pycor >= 10  
  [set GAV 14]  
  if pycor < 10 and pycor >= 8  
  [set GAV 13]  
  if pycor < 8 and pycor >= 6
```

```

[set GAV 12]
if pycor < 6 and pycor >= 4
[set GAV 11]
if pycor < 4 and pycor >= 2
[set GAV 10]
if pycor < 2 and pycor >= 0
[set GAV 9]
if pycor < 0 and pycor >= -2
[set GAV 8]
if pycor < -2 and pycor >= -4
[set GAV 7]
if pycor < -4 and pycor >= -6
[set GAV 6]
if pycor < -6 and pycor >= -8
[set GAV 5]
  if pycor < -8 and pycor >= -10
[set GAV 4]
if pycor < -10 and pycor >= -12
[set GAV 3]
if pycor < -12 and pycor >= -14
[set GAV 2]
if pycor < -14 and pycor >= -16
[set GAV 1]
end

```

to setup-soil

```

set soil 0
ask patches
  [set pcolor green
  if pycor < -1
  [ set pcolor black ]]
end

```

to exc-face

```

ask patch 0 -1 [set pcolor red]
set branches 1
end

```



```

to setup-turtles
  create-turtles population
  [ set color yellow ]
  set-default-shape turtles "bug"
  ask turtles [ setxy random-xcor -15 ]
end

to go
  ask turtles [
    roaming
    excavating
    depositing
  ]
  tick
end

to roaming
  if GAV >= 3 [
    if pcolor = black [
      rt random 90 ; set random heading
      lt random 90
      forward 1]
    if GAV >= 8
      [if count turtles in-radius 1 with [color = red] > 0
      [ set color orange
      wait CWP
      if count turtles in-radius 1 with [color = red] > 0
      [ set heading 90
      ask patch-at 1 0 [set pcolor red]
      set soil soil + 1
      set branches branches + 1]
      excavating]]]
  if GAV < 3
    [ if pcolor = black [
      rt random 90 ; set random heading
      lt random 90
      forward 1]
      if pcolor = green [

```

```

        rt random 90 ; set random heading
        lt random 90
        forward 1]]
;   if GAV < 8
;   [ set color yellow]
;   if count turtles in-radius 1 with [color = orange] > 0
;   [ set color orange
;   wait CWP
;   roaming]
end

```

to excavating

```

if pcolor = red [
    set color red
    set pcolor black
    set soil soil + 1
    wait 0.25
    set heading 180 ; But is there a way to get red ants to never pick up?
    ask patch-at 0 1 [set pcolor red]
    forward 1
    depositing]
if pcolor = green [
    back 1]
end

```

to depositing

```

if color = red ;or color = orange
[downhill GAV
if GAV < 3
    [if pcolor = black
        [set pcolor green
        set color yellow
        roaming]
    if pcolor = green ;How will we make sure that the depository area doesn't get blocked off
for the agents?
    [ rt random 90 ; set random heading
        lt random 90
        forward 1]]]

```

```
; set pcolor green
; set color yellow
; roaming]]
end
```

to-report sand-excavated

```
;report count patches with [pcolor = green] with [GAV < 3]
report soil
plot sand-excavated
end
```

to-report branches-formed

```
; report count patches with [pcolor = red]
report branches
plot branches-formed
end
```

APPENDIX B

ARDUINO CODE

```
#include <Servo.h>

int BIN_1 = 11;
int BIN_2 =10;
int AIN_1 = 5;
int AIN_2 =6;
const int ledforce=9;
#define iruno 8
#define laser A3
const int FSR_PIN=A2;
Servo myservo;

void setup() {
  // put your setup code here, to run once:
  pinMode(BIN_1, OUTPUT);
  pinMode(BIN_2, OUTPUT);
  analogReference(DEFAULT);
  pinMode(AIN_1, OUTPUT);
  pinMode(AIN_2, OUTPUT);
  pinMode(iruno, INPUT);
  pinMode(laser, INPUT);
  pinMode(FSR_PIN, INPUT);
  pinMode(ledforce, OUTPUT);
  myservo.attach(A5);
}

void loop() {
  int fsrADC=analogRead(FSR_PIN);
  int raw=analogRead(iruno);
  int top=analogRead(laser);

  if iruno>(400){
    myservo.write(120);
    digitalWrite(AIN_1,HIGH);
    digitalWrite(BIN_1,HIGH);
    digitalWrite(AIN_2,LOW);
    digitalWrite(BIN_2,LOW);}

  if iruno<=(400){
```

```

if irtop =0{
digitalWrite(AIN_1,LOW);
digitalWrite(BIN_1,LOW);
digitalWrite(AIN_2,LOW);
digitalWrite(BIN_2,LOW);
delay(2000);
digitalWrite(AIN_1,LOW);
digitalWrite(BIN_1,LOW);
digitalWrite(AIN_2,HIGH);
digitalWrite(BIN_2,HIGH)};
if FSR_PIN>=(800){
digitalWrite(AIN_1,LOW);
digitalWrite(BIN_1,LOW);
digitalWrite(AIN_2,LOW);
digitalWrite(BIN_2,LOW);
digitalWrite(ledforce,HIGH);
digitalWrite(AIN_1,HIGH);
digitalWrite(BIN_1,LOW);
digitalWrite(AIN_2,LOW);
digitalWrite(BIN_2,LOW);}
if iruno>=(400){
digitalWrite(AIN_1,HIGH);
digitalWrite(BIN_1,HIGH);
digitalWrite(AIN_2,LOW);
digitalWrite(BIN_2,LOW);
if irtop =1{
delay(100000)
digitalWrite(AIN_1,LOW);
digitalWrite(BIN_1,LOW);
digitalWrite(AIN_2,LOW);
digitalWrite(BIN_2,LOW);
delay(2000);
digitalWrite(AIN_1,LOW);
digitalWrite(BIN_1,LOW);
digitalWrite(AIN_2,HIGH);
digitalWrite(BIN_2,HIGH)};
if FSR_PIN>=(800){
digitalWrite(AIN_1,LOW);

```

```
digitalWrite(BIN_1, LOW);  
digitalWrite(AIN_2, LOW);  
digitalWrite(BIN_2, LOW);  
digitalWrite(ledforce, HIGH);  
digitalWrite(AIN_1, HIGH);  
digitalWrite(BIN_1, LOW);  
digitalWrite(AIN_2, LOW);  
digitalWrite(BIN_2, LOW);} }  
}
```

```
if iruno<=(400){  
digitalWrite(AIN_1, LOW);  
digitalWrite(BIN_1, HIGH);  
digitalWrite(AIN_2, LOW);  
digitalWrite(BIN_2, LOW);  
delay(4000);  
myservo.write(55);  
digitalWrite(ledforce, LOW);  
digitalWrite(AIN_1, LOW);  
digitalWrite(BIN_1, LOW);  
digitalWrite(AIN_2, LOW);  
digitalWrite(BIN_2, LOW);  
delay(2000);  
digitalWrite(AIN_1, HIGH);  
digitalWrite(BIN_1, HIGH);  
digitalWrite(AIN_2, LOW);  
digitalWrite(BIN_2, LOW);} }
```

```
myservo.write(120);  
digitalWrite(AIN_1, LOW);  
digitalWrite(BIN_1, LOW);  
digitalWrite(AIN_2, LOW);  
digitalWrite(BIN_2, LOW);  
delay(2000);  
}
```